Pathogenic NLRP3 mutants forms constitutively active inflammasomes resulting in immune-metabolic limitation of IL-1β production

Cristina Molina-López[1], Laura Hurtado-Navarro[1], Carlos J. García[2], Diego Angosto-Bazarra[1], Fernando Vallejo[2], Ana Tapia-Abellán[1,9], Joana R. Marques-Soares[3], Carmen Vargas[4], Segundo Bujan-Rivas[3], Francisco A. Tomás-Barberán[2], Juan I. Arostegui[5,6,7] and Pablo Pelegrin[1,8]

[1]Molecular Inflammation Group, Instituto Murciano de Investigación Biosanitaria Pascual Parrilla–IMIB, Murcia, Spain

[2]Quality, Safety and Bioactivity of Plant-Derived Foods, Centro de Edafología y Biología Aplicada del Segura-Consejo Superior de Investigaciones Científicas (CEBAS-CSIC), Murcia, Spain

[3]Department of Internal Medicine, Hospital Vall Hebron, Barcelona, Spain

[4]Department of Rheumatology, Hospital Virgen de la Macarena, Sevilla, Spain

[5]Department of Immunology, Hospital Clínic, Barcelona, Spain

[6]Institut d'Investigacions Biomèdiques August Pi i Sunyer, Barcelona, Spain

[7]School of Medicine, Universitat de Barcelona, Barcelona, Spain

[8]Department of Biochemistry and Molecular Biology B and Immunology, Faculty of Medicine, University of Murcia, 30120 Murcia, Spain

[9]Present address: Interfaculty Institute for Cell Biology, Department of Immunology, University of Tübingen, Auf der Morgenstelle 15, 72076 Tübingen, Germany.

Corresponding author: Dr. Pablo Pelegrín. Edificio LAIB 4ª Planta, Campus Ciencias de la Salud. Universidad de Murcia. Carretera Buenavista s/n. 30120 El Palmar, Murcia, Spain. Phone: +34 868 885 038; e-mail: pablopel@um.es

Brief title: Constitutively active pathogenic inflammasome modify immunometabolism

ABSTRACT

Cryopyrin-associated periodic syndrome (CAPS) is an autoinflammatory condition resulting from monoallelic *NLRP3* variants that facilitate IL-1β production. Although these are gain-of-function variants characterised by hypersensitivity to cell priming, patients with CAPS and animal models of the disease may present inflammatory flares without identifiable external triggers. Here we find that CAPS-associated NLRP3 variants are forming constitutively active inflammasome, which induce increased basal cleavage of gasdermin D, IL-18 release and pyroptosis, with a concurrent basal pro-inflammatory gene expression signature, including the induction of nuclear receptors 4A. The constitutively active NLRP3-inflammasome is responsive to the selective NLRP3 inflammasome inhibitor MCC950 and its activation is regulated by deubiquitination. Despite their preactivated state, the CAPS inflammasomes are responsive to activation of the NF-κB pathway. NLRP3-inflammasomes with CAPS-associated variants affect the immunometabolism of the myeloid compartment, leading to disruptions in lipids and amino acid pathways and impaired glycolysis, limiting IL-1β production. In summary, NLRP3 variants causing CAPS form a constitutively active inflammasome inducing pyroptosis and IL-18 release without cell priming, which enables the host's innate defence against pathogens while also limiting IL-1β–dependent inflammatory episodes through immunometabolism modulation.

Key words: Autoinflammatory disease; NLRP3; CAPS; inflammasome; deubiquitination; metabolism; glycolysis.

INTRODUCTION

The Nucleotide-binding oligomerization domain, leucine-rich repeat receptor, and pyrin-domain containing-protein 3 (NLRP3) inflammasome is a multiprotein cytosolic complex involved in different human inflammatory diseases [1]. The NLRP3-inflammasome triggers the activation of caspase-1, which in turn processes several proteins within the cell, including gasdermin D (GSDMD) and the pro-inflammatory cytokines interleukin (IL)-1β and IL-18. The amino-terminal fragment of GSDMD inserts itself into the plasma membrane, oligomerizes and forms pores, which facilitate the release of IL-1β and IL-18, and initiate a specific type of cell death known as pyroptosis [2]. Rare variants in the *NLRP3* gene are responsible for a monogenic autoinflammatory disease called Cryopyrin-associated periodic syndrome (CAPS) [3,4]. CAPS includes three different clinical phenotypes with increasing severity: familial cold autoinflammatory syndrome (FCAS) as the mildest form, the Muckle–Wells syndrome (MWS) as the intermediate phenotype, and the neonatal-onset multisystem inflammatory disease/chronic infantile neurologic cutaneous articular syndrome (NOMID/CINCA) as the most severe expression [4,5]. Typically, these phenotypes manifest early in life and are characterized by recurrent episodes of fever, urticaria-like skin rashes, conjunctivitis, and joint inflammation. From a genetic point of view, most CAPS patients carry germline *NLRP3* variants, with a smaller group carrying post-zygotic variants [6–8]. While specific *NLRP3* variants have been associated with each CAPS clinical phenotype, current understanding suggests that some *NLRP3* variants may cause overlapping phenotypes. This supports the idea that CAPS behaves more like a syndrome with a variable spectrum of features rather than a singular entity [5].

While *NLRP3* variants associated with CAPS are typically considered gain-of-function due to their dominant phenotype, most *in vitro* studies rely on the bacterial trigger lipopolysaccharide (LPS) to induce the activation of these inflammasomes. This activation is then detected by the release of IL-1β [9–16]. The canonical activation of the

wild type NLRP3 inflammasome requires two sequential steps. The first step, or priming, induces nuclear factor (NF)-κB activation and transcriptional expression of *NLRP3* and *IL1B*. It also promotes key NLRP3 post-transcriptional modifications, notably deubiquitination [17,18]. The second step relies on cellular stress inducers, such as the decrease of intracellular K^+ by the ionophore nigericin or the activation of the cationic P2X7 receptor. Both of these triggers cause a conformational change in the NLRP3 inactive structure [19,20]. Therefore, NLRP3 with gain-of-function variants may only require priming to assemble an active inflammasome, rendering it hypersensitive. However, is not well understood how the CAPS-associated NLRP3 inflammasome is triggered in patients with CAPS and knock-in CAPS animal models that develop spontaneous systemic inflammatory responses from birth onwards in the absence of infection [21]. Recombinant expression of CAPS-associated *NLRP3* variants results in an open structure that favours inflammasome formation accompanied by a constitutive puncta distribution within the cell [22,23].

One challenge in studying gain-of-function *NLRP3* variants is the difficulty in distinguishing between the priming signal and the *NLRP3* expression *per se*. In this study, we use an inducible cellular system to express different gain-of-function *NLRP3* variants independently of the priming signal. We show that expression of CAPS-associated NLRP3 variants result in a constitutively active inflammasome that is regulated by ubiquitination. This results in a basal inflammatory programming and alter immunometabolism that limit IL-1β, but not IL-18 production. Therefore inflammatory flares in CAPS are controlled by glycolysis impairment, while maintaining a basal inflammatory programme as a defence mechanism against pathogens.

RESULTS

CAPS-associated NLRP3 variants result in a constitutively active inflammasome

We initially analysed blood samples from patients with CAPS carrying the germline pathogenic NLRP3 variants p.R260W, p.D303N, p.T348M and p.A439T [24]. Culturing whole blood from these patients without any stimulation resulted in an increased percentage of monocytes with ASC specks, used as a hallmark of inflammasome activation, when compared to healthy individuals (**Figure 1A**). LPS stimulation further enhanced the percentage of ASC-specking monocytes in both groups, although this increase was less pronounced in healthy controls (**Figure 1A**). In contrast, treatment with the NLRP3 inhibitor MCC950 (a.k.a. CRID3 or CP-456773) reduced the percentage of ASC-specking monocytes in both groups, with a marked reduction in CAPS patients (**Supplementary Figure 1**). These results suggest that monocytes from CAPS patients exhibit constitutive NLRP3-inflammasome activation. Consistent with this, unstimulated peripheral blood mononuclear cells (PBMCs) from CAPS patients showed a constitutive release of the pyroptotic marker galectin-3 and the cytokine IL-18 (**Figure 1B,C**), with no detectable basal release of IL-1β or TNF-α (**Figure 1D,E**). LPS stimulation led to an enhanced IL-1β release from the patients' PBMCs, but not from the healthy individuals (**Figure 1D**), because is known that LPS is required for the transcriptional upregulation of IL-1β. We also found that LPS slightly, but significantly, increased the release of both IL-1β and IL-18 from the PBMCs of healthy individuals: IL-18 concentration increased from 0.78±0.13 pg/ml at 6h resting to 2.18±0.52 pg/ml after 6h of LPS treatment, with a *t*-test *p*-value of 0.0296; and IL-1β concentration increased from 0.65±0.28 pg/ml at 4h resting to 11.09±2.57 pg/ml after 4h of LPS treatment, with a *t*-test *p*-value of 0.0037 (**Figure 1C,D**). However, this increase was less pronounced than that observed in the PBMCs of CAPS patients. This corresponds to the observed increase in ASC specks following LPS incubation in monocytes from healthy donors (**Figure 1A**). We also observed a genotype-dependent differential release of galectin-3 and IL-1β, being higher

in patients carrying the p.A439T variant compared to those carrying the remaining NLRP3 variants (**Figure 1B,D**). Nevertheless, the observed increase in the percentage of ASC-specking monocytes was consistent across all analysed variants (**Figure 1A**). This observation raises an intriguing hypothesis, while different NLRP3 variants may prompt constitutive inflammasome assembly, subsequent downstream signalling could be distinctly regulated. To investigate the effect of LPS stimulation on human monocyte activation, we analysed the GEO dataset GSE42606. The analysis revealed that LPS upregulates the expression of *IL1B*, *TNFA,* and *NLRP3* in healthy human PBMCs, while the expression of *IL18* and *LGALS3* remains unchanged (**Figure 1F**). Contrarily, in active CAPS patients carrying the p.G569R NLRP3 variant, no discernible alteration in the expression patterns of *IL1B*, *IL18* and *NLRP3* in blood cells was observed, according to the analysis of GEO dataset GSE57253 (**Figure 1G**). These findings collectively point towards the likelihood of an inherent constitutively NLRP3-inflammasome activation mechanism within CAPS.

Expression levels of NLRP3 pathogenic variants condition the constitutive activation of the inflammasome

To investigate the activation of pathogenic NLRP3 variants independently of the NLRP3 inflammasome priming signal, we employed an inducible recombinant system in NLRP3-deficient immortalized mouse macrophages, where human *NLRP3* expression is regulated by doxycycline [22,25]. Inducing the expression of NLRP3 carrying the CAPS-associated variants p.R260W, p.T348M, and p.D303N, excluding the wild type, led to a constitutive processing of GSDMD (**Figure 2A**). By increasing the concentration of doxycycline, we were able to enhance the expression level of mutant NLRP3, leading to increased GSDMD processing (**Figure 2A, Supplementary Fig. 2A**). GSDMD processing was found to be dependent on NLRP3 activity, as evidenced by observing a reduction in GSDMD cleavage following treatment with the NLRP3 inhibitor MCC950 (**Figure 2A**). Blocking GSDMD processing with MCC950 led to an increase in the

155 expression of CAPS-associated NLRP3 variants in macrophages (**Figure 2A**), probably
156 due to the increase of *NLRP3* gene expression by non-dying cells. Moreover, by using
157 different doxycycline doses to achieve similar expression levels of both the wild type and
158 p.D303N NLRP3, GSDMD cleavage was exclusively observed in macrophages
159 expressing the mutant NLRP3 variant (**Supplementary Fig. 2B**). Therefore, to compare
160 the function of wild type and p.D303N NLRP3 at similar expression levels, these varying
161 concentrations of doxycycline were used in subsequent experiments. Alongside GSDMD
162 processing, NLRP3 p.D303N expression also led to caspase-1 activation (**Figure 2B**), a
163 heightened percentage of macrophages forming ASC oligomers (**Figure 2C,**
164 **Supplementary Fig. 2C**), and pyroptosis induction (**Figure 2D**). We also observed that
165 different CAPS-associated NLRP3 variants triggered the release of the constitutively
166 expressed cytokine IL-18, which was inhibited by MCC950 (**Figure 2E**). However,
167 MCC950 presented a less potent inhibitory effect on the NLRP3 p.T348M variant,
168 affecting both GSDMD processing and IL-18 release (**Figure 2A,E**). This observation
169 aligns with a prior report indicating higher IC_{50} for MCC950 in PBMCs from CAPS
170 patients carrying the p.T348M variant compared to the p.A439V and p.E311K variants [9].
171 Furthermore, in recombinant systems, MCC950 was unable to completely eliminate cells
172 with NLRP3 p.T348M-associated puncta [22]. These findings suggest that therapy
173 strategies involving MCC950 analogues might require dosage adjustments based on the
174 specific *NLRP3* variant carried by patients.
175 The expression of the p.D303N NLRP3 variant was found to increase with the duration
176 of doxycycline incubation (**Figure 3A**). Interestingly, this increase was not observed
177 during extended incubation periods with doxycycline (16 h), likely due to the induction of
178 pyroptosis. By contrast, blocking constitutive NLRP3 activation with MCC950 led to a
179 sustained high expression of NLRP3 p.D303N, even during prolonged doxycycline
180 exposure (**Figure 3A**). These findings suggest that viable cells may promote the
181 accumulation of inhibited NLRP3 p.D303N. Concurrently, augmented mutant NLRP3
182 expression triggered parallel GSDMD processing, LDH, and IL-18 release (**Figure 3A-**

C). To verify that the expression of CAPS-associated NLRP3 variants result in a constitutively active inflammasome, we conducted a single–cell analysis using flow cytometry and Time of Flight for Inflammasome Evaluation (TOFIE) in HEK293T. This revealed an increased percentage of cells with ASC oligomers when the mutant p.D303N NLRP3 was equivalently expressed to the wild type NLRP3 (**Figure 3D, Supplementary Fig. 2D**). In an attempt to mimic the typical heterozygous genotype of CAPS patients, we co-expressed both wild type and p.D303N NLRP3 in the same cells (**Supplementary Fig. 2E**). Data showed that the wild type NLRP3 induced a significant increase in cells with ASC oligomers at low p.D303N NLRP3 expression levels, but not at high levels (**Figure 3D**). This suggests that even low concentrations of mutant NLRP3 can enable the wild type to potentially intensify the basal autoactivation of the mutant NLRP3 inflammasome. This results in the oligomerization of ASC, caspase-1 activation, and GSDMD processing, all occurring independently of any priming signal. These results align with previous observation that CAPS-associated NLRP3 variants inherently display an open active structure and a constitutive puncta distribution within the cell without external stimulation [22].

NF-κB induction modulates the secretome of pathogenic NLRP3 variants

Consistent with the results obtained from monocytes analysis of CAPS patients as shown in Figure 1, the expression of pathogenic NLRP3 variants in immortalized macrophages did not trigger a significant release of IL-1β. As expected, IL-1β release was strongly induced following LPS treatment (**Figure 3E**). LPS also promoted the release of TNF-α, which was independent of the expression of p.D303N NLRP3 variant, as evidenced by the fact that MCC950 did not modify TNF-α release but completely inhibited IL-1β release (**Figure 3E,F**). Interestingly, LPS stimulation also enhanced IL-18 release and GSDMD cleavage when the p.D303N NLRP3 variant was expressed (**Figure 3A,C**). Aligning with this observation, other NF-κB activators, such as palmitate, S100A9 or IL-6 acted as

inductors of NLRP3-dependent IL-1β release when pathogenic NLRP3 variants p.R260W, p.D303N and p.T348M were expressed, which was not the case with the expression of the wild type allele (**Figure 4A, Supplementary Fig. 3A-C**). For control, wild type NLRP3 expression induced IL-1β release following LPS and nigericin treatment (**Supplementary Fig. 3D**). Additionally, palmitate, S100A9 and IL-6 induced TNF-α release regardless of the expressed NLRP3 variants (**Figure 4B**). These compounds were all able to activate NF-κB in a macrophage reporter system (**Figure 4C**). As expected, MCC950 inhibited IL-1β release from macrophages expressing the p.D303N NLRP3 variant, but did not affect TNF-α production (**Figure 4A,B**). Furthermore, the TLR agonists LPS and Pam3-CSK_4 also triggered IL-1β release from macrophages expressing the pathogenic NLRP3 variants (**Figure 4A**), and were also capable of inducing NF-κB and TNF-α release (**Figure 4B,C**). Notably, the p.T348M NLRP3 variant exhibited a subdued IL-1β release compared to the p.R260W and p.D303N NLRP3 variants (**Figure 4A**). Both palmitate and IL-6 were more effective in inducing IL-1β release when the p.D303N NLRP3 variant was expressed (**Figure 4A**).

The stimulation of whole blood from CAPS patients with palmitate, S100A9, IL-6 and Pam3-CSK_4 led to an increase in the percentage of ASC-specking monocytes. However, this increase was less pronounced in equally treated monocytes from healthy individuals (**Figure 4D**). IL-1β release from CAPS PBMCs was triggered after stimulation with palmitate, S100A9 and Pam3-CSK_4, whereas unstimulated cells or those treated with recombinant IL-6 did not elicit this response (**Figure 4E**). Serving as control, TNF-α release was also induced in PBMCs from both CAPS patients and healthy individuals treated with palmitate, S100A9 and Pam3-CSK_4, but not by IL-6 (**Figure 4F**). This absence of response may stem from IL-6 inability to activate the NF-κB pathway in samples from CAPS patients. Further examination of the GEO dataset GSE57253 revealed increased *S100A9* gene expression in blood cells from active CAPS patients when compared to healthy donors (**Figure 4G**). Remarkably, anakinra treatment in

CAPS patients reduced *S100A9* gene expression (**Figure 4G**). This suggests that alarmins, such as S100A9, could be involved in CAPS flares by enhancing the activity of the mutant NLRP3 inflammasome.

Triggers of the canonical wild type NLRP3 inflammasome, such as extracellular adenosine 5'-triphosphate (ATP) or monosodium urate (MSU) crystals failed to induce IL-1β release from immortalized macrophages expressing the pathogenic NLRP3 variants (**Figure 4A**), as these compounds were unable to activate NF-κB (**Figure 4C**). We observed a dose-dependent release of IL-1β from macrophages expressing the p.D303N NLRP3 variant upon exposure to increasing concentrations of palmitate, S100A9, IL-6, LPS and Pam3-CSK_4 (**Supplementary Fig. 3A**), similar to the TNF-α release pattern (**Supplementary Fig. 3A**). However, there was a noticeable delay in the release kinetics of IL-1β in comparison to TNF-α release (**Supplementary Fig. 3B**). This underscores the dependency of IL-1β release in pathogenic NLRP3 variants on two distinct processes: initially the by NF-κB pathway stimulates the expression of pro-IL-1β (**Supplementary Fig. 3C**), which is then followed by its cleavage and release due to the constitutively active pathogenic NLRP3 inflammasome.

Given our observation of increased GSDMD cleavage and IL-18 release after LPS stimulation (**Figure 3A,B**), we aimed to investigate the possibility of NF-κB activation modulating the constitutively active p.D303N NLRP3 inflammasome. We found a slight increased processing of caspase-1 p20 and GSDMD processing following NF-κB induction with palmitate, S100A9, IL-6, LPS and Pam3-CSK_4 (**Figure 5A**). Consistently, treatment of macrophages expressing the p.D303N NLRP3 variant with these compounds resulted in a significant increase in ASC specking macrophages (**Figure 5B**), as well as IL-18 and IL-1α release (**Figure 5C,D**), P2X7 receptor shedding (**Figure 5E**), and pyroptosis (**Figure 5F**). As expected, MCC950 was able to reduce all these effects (**Figure 5C-F**). These data suggest that while IL-1β release was strongly

dependent on NF-κB induction, the constitutive activity of the mutant NLRP3 inflammasome was slightly modulated by NF-κB at a constant NLRP3 expression.

NF-κB activation from macrophages expressing the p.D303N NLRP3 variant was also crucial for the inflammasome-dependent release of HMGB1 and cystatin B (**Supplementary Fig. 4A,B**), with palmitate being the weakest inducer (**Supplementary Fig. 4A,B**) and the weakest NF-κB activator (**Figure 4C**). In contrast, the pathogenic p.D303N NLRP3 variant was not implicated in the release of cathepsin B, CD14, CD206 or annexin A1 (**Supplementary Fig. 4C-F**), which were previously identified to be released upon canonical inflammasome activation by extracellular ATP [26].

Ubiquitin regulates the basal activity of mutant NLRP3 inflammasome

Deubiquitinases (DUBs) are known to play a role in the priming and activation of the canonical wild type NLRP3 inflammasome [27]. Consequently, we next aimed to investigate whether DUBs could also be regulating the activity of the mutant NLRP3 inflammasome. The application of broad-spectrum DUBs inhibitors, G5 and PR-619, in macrophages expressing the p.D303N NLRP3 variant resulted in a reduction of GSDMD processing (**Figure 6A**) and IL-18 release (**Figure 6B**). Similarly, the administration of the selective USP14 and UCHL5 inhibitor, b-AP15, also led to a decrease in GSDMD processing and IL-18 release (**Figure 6A,B**), thus suggesting that deubiquitination of the mutant NLRP3 may favour the constitutive activation of the CAPS-related inflammasome. Moreover, the different DUB inhibitors were also capable of reducing GSDMD processing following LPS treatment of macrophages expressing the p.D303N NLRP3 variant (**Figure 6C**), without impacting LPS-induced NF-κB activation in the NF-κB reporter Raw264.7 cells (**Figure 6D**) or TNF-α release (**Figure 6E**). In the presence of LPS, the different DUB inhibitors further decreased the release of inflammasome-dependent cytokines IL-18 and IL-1β (**Figure 6F,G**). Notably, both G5 and b-AP15 exhibited a mild reductive effect on the percentage of ASC-specking monocytes in

untreated blood samples from CAPS patients, with this decline being more pronounced in LPS-treated blood samples (**Figure 6H**). Although NF-κB activation was not affected by the DUB inhibitors (**Figure 6D**), we discerned that all employed DUB inhibitors (G5, PR-619 and b-AP15) induced a significant decrease in LPS-induced *Il1b* and *Il18* gene expression, without affecting the expression of *Tnfa*, *Pycard*, *Casp1*, *Gsdmd*, *Nek7* or *Nlrp3* (**Supplementary Fig. 5**). This suggests that DUBs might be modulating mutant NLRP3 inflammasome activity beyond merely influencing *Il1b* and *Il18* gene expression. Collectively, our data indicates that DUBs control the constitutive activation of the CAPS-associated NLRP3-inflammasome, as observed in both circulating monocytes from CAPS patients and immortalized macrophages recombinantly expressing pathogenic NLRP3 variants.

Constitutive active mutant NLRP3 inflammasome induces metabolic reprogramming

Given that an inflammatory state can rapidly shift oxidative metabolism towards glycolysis [28,29], we next aimed to evaluate whether the constitutive active mutant NLRP3-inflammasome could impact the metabolism of myeloid cells. For this purpose, monocytes isolated from healthy individuals or CAPS patients carrying the pathogenic p.A439T NLRP3 variant, either unstimulated or treated with LPS, underwent untargeted metabolomics analysis. The pre-processing of the entire metabolite dataset resulted in a data matrix comprising 203 metabolites in negative polarity and 925 in positive polarity, from which they were reduced to 603 metabolites in positive polarity after removal metabolites with high variability among replicates (**Supplementary Data 1**). To efficiently represent the variability of these metabolites among monocytes of healthy donors and CAPS patients while preserving trends and patterns, we employed a principal component analysis (PCA) model on the final merged data matrix (**Figure 7A**). The calculated PCA model was built based on 16 samples and three components, with the first two principal components (PC1 and PC2) accounting for 25.2% and 9.6% of the overall variability,

respectively. PCA model results illustrated variations based on the total covariance among the study cohorts. We observed that the metabolomic variation of the untreated monocytes from CAPS patients clustered more closely with the LPS-treated monocytes from healthy individuals (**Figure 7A**), suggesting an inherent pro-inflammatory profile of CAPS monocytes. In fact, both unstimulated monocytes from CAPS patients and those from healthy donors treated with LPS were mainly explained by component 1, indicating that the differences evidenced in sample metabolomes might be influenced by these variables. This observation was further confirmed, as 423 metabolites displayed differential presence in monocytes from healthy individuals and CAPS patients (**Figure 7B**). Of these, 46 were found to be upregulated in LPS-treated monocytes from healthy donors. Interestingly, these same metabolites were also found to be upregulated in both untreated and LPS-treated monocytes from CAPS patients, when compared to untreated monocytes from healthy donors (**Figure 7B**). Subsequently, 121 metabolites were observed to be upregulated, while 256 metabolites were found to be downregulated in monocytes from CAPS when compared to monocytes from healthy individuals (**Figure 7B**). Volcano plots further revealed significant differences in the metabolites when contrasting monocytes from CAPS patients with those from healthy donors, both under resting conditions and post-LPS treatment (**Figure 7C**). Aligning with the pro-inflammatory metabolomic landscape of the monocytes from CAPS patients, differences in metabolites were less pronounced when comparing untreated monocytes from CAPS patients with LPS-treated monocytes from healthy individuals (**Supplementary Fig. 6A**). The untargeted metabolomics analysis conducted was not sufficiently conclusive in identifying the metabolites that varied between monocytes from healthy individuals and those from CAPS patients, due to limited sample availability for the targeted MS/MS analysis required for metabolite confirmation through spectra fragmentation patterns. However, we managed to tentatively identify 14 metabolites, with an error rate ranging from -2.68 to 8.52 ppm, which exhibited differential presence in monocytes of the two groups (**Supplementary Table 2, Supplementary Fig. 6B**). These included lipids and

lipid-like molecules, as well as amino acids and their synthesis intermediates, most of which were derived from glycolysis intermediates (**Supplementary Table 2, Supplementary Fig. 6B**).

To further validate changes in metabolites associated with the auto-active mutant NLRP3 inflammasome, we conducted an untargeted metabolomics analysis in immortalized macrophages expressing the pathogenic p.D303N NLRP3 variant. The pre-processing operations from the full metabolites data set yielded a data matrix based on 243 metabolites and 636 metabolites in negative and positive polarities respectively (**Supplementary Data 2**), with 166 metabolites upregulated in immortalized macrophages expressing mutant NLRP3. The calculated PCA model was constructed based on 12 samples and three components. The PC1 and PC2 accounted for 29.5% and 15.9% of the total variability respectively, and indicated that the macrophages expressing NLRP3 p.D303N variant formed a group that was similar to the LPS-treated macrophages that were not expressing NLRP3 (**Supplementary Fig. 6C**). A tentative identification of 17 metabolites, with an error rate ranging from -2.69 to 8.87 ppm, were also found to be enriched in lipids, amino acid and their derivative/intermediate metabolites (**Supplementary Table 3, Supplementary Fig. 6B**). This confirms that the expression of pathogenic NLRP3 variants affects distinct metabolic pathway in CAPS monocytes.

Glycolysis is impaired by the active mutant NLRP3 inflammasome

We then proceeded to examine the expression of metabolic-associated gene expression in two independent GEO datasets (GSE57253 and GSE17732) that included blood samples obtained from CAPS patients during an active disease periods [30,31]. Interestingly, our analysis revealed a marked differential expression of genes associated with glycolysis and the pentose phosphate pathway in blood cells of active CAPS patients. Moreover, upon patients treatment with IL-1 inhibitor anakinra, the expression of these genes appear to normalize (**Figure 7D, Supplementary Fig. 7A**). Genes

associated with pentose phosphate (*DERA, PGM2, NAMPT*) and glycolysis (*BPGM, LDHA, PFKFB3*) revealed elevated expression in blood cells from active CAPS patients, and a decrease following anakinra treatment (**Figure 7D, Supplementary Fig. 7A**). In contrast, the expression of the glycolytic enzyme encoded by the *ENO3* gene tended to decrease during active CAPS and was restored following anakinra treatment (**Figure 7D, Supplementary Fig. 7A**). A similar gene expression assessment in immortalized macrophages expressing the mutant p.D303N NLRP3 induced by doxycycline, revealed a predominant upregulation trend for genes associated with the pentose phosphate pathway (**Figure 7E**), contrasting with a downregulation for the glycolytic-related genes (**Figure 7E**). This discrepancy might be because in the case of CAPS patients, the blood samples for these studies were drawn during an inflammatory flare, whereas immortalized macrophages were unprimed and had not encountered any pro-inflammatory stimuli. Indeed, when CAPS patients were treated with anakinra, the same induced downregulation in glycolytic gene expression as was found, mirroring the findings seen when the p.D303N NLRP3 was expressed in immortalized macrophages (**Figure 7D,E**). A full analysis of RNA sequencing of immortalized macrophages expressing the p.D303N NLRP3 variant showed that most of the glycolytic genes were down-regulated and their expression was recovered with MCC950 treatment (**Figure 8A,B**). Expression of the wild type NLRP3 in immortalized macrophages did not significantly influence the expression of glycolytic genes (**Figure 8B**). On the contrary, genes associated with the pentose phosphate pathway clustered with those that were upregulated upon expression of p.D303N NLRP3 (**Figure 8A, Supplementary Fig. 7B**). This group also included genes related to the inflammatory response, apoptosis, lipid and amino acid metabolism, immune responses to virus, oxidative stress and IL-17 (**Figure 8A,C, Supplementary Table 4**). This underlines that CAPS exhibit changes in lipids, amino acids and associated intermediates, along with a basal inflammatory state, potentially enhancing the ability to counteract pathogens (since cellular pathways related to virus response were significantly enriched). Among inflammatory genes, we detected

upregulation of the nuclear receptors 4A1 and 4A2, key for the activation of an inflammatory program in macrophages. When analysing biological processes downregulated upon p.D303N NLRP3 expression and restored with MCC950 treatment, we identified pathways related to cellular homeostatic functions and tissue regeneration, including transcription, cell proliferation, cytoskeleton organization, angiogenesis regulation, cell migration or ERK cascades (**Figure 8C, Supplementary Table 5**). Importantly, genes associated to hypoxic responses and the metabolism of lipids and carbohydrates were down regulated upon the expression of the mutant p.D303N NLRP3 (**Figure 8C, Supplementary Table 5**).

To further investigate whether alterations in gene expression led to functional changes in macrophages expressing either mutant or wild-type NLRP3, we examined glycolysis functionality. To achieve this, we evaluated glycolysis rate by measuring the acidification of extracellular media produced by mitochondria in response to proton efflux and measured the oxygen consumption rate of these macrophages. Our results indicated that macrophages expressing the mutant NLRP3 variant displayed decreased basal and compensatory glycolysis (following mitochondrial respiration inhibition), regardless of whether they were treated with LPS or not (**Figure 9A,B**). Administrating MCC950 restored the glycolytic activity of the macrophages expressing the mutant p.D303N NLRP3 (**Figure 9A,B**), simultaneously to an upregulation in glycolytic-related gene expression (**Figure 8B**). Neither doxycycline nor MCC950 had any effect in the glycolysis of *Nlrp3*$^{-/-}$ macrophages infected with the empty vector virus, or in macrophages expressing wild type NLRP3 (**Figure 9B**). The reduction in glycolysis was a result of the p.D303N NLRP3 inflammasome activity, as it was reversed by MCC950 (**Figure 9A,B**). However, this effect was not due to IL-1 downstream signalling, as the glycolytic rate remained unaffected when incubated with recombinant IL-1Ra (**Supplementary Fig. 7C**). Furthermore, there was a noticeable decrease in the production of lactate, pyruvate, and glycolytic ATP when the mutant NLRP3 was expressed, and this reduction was mitigated upon administering MCC950 (**Figure 9C,D, Supplementary Fig. 8A**). Even

though the expression of mutant NLRP3 also influenced mitochondrial ATP production (**Figure 9D**), it did not alter mitochondrial basal or maximal respiration in resting macrophages, while slightly decreasing in LPS-treated macrophages (**Figure 9E, Supplementary Fig. 8B**). Similarly, metabolites from the tricarboxylic acid cycle such as citrate, malate, fumarate, succinate, and ketoglutarate, along with their associated genes, remained unchanged after the expression of the p.D303N NLRP3 variant (**Supplementary Fig. 8C,D**).

Glycolysis impairment due to constitutive active mutant NLRP3 inflammasome limit basal IL-1β production

To gain insights into the functional consequences of the decreased of glycolysis associated with pathogenic NLRP3 variants, we supplemented immortalized macrophages cultures expressing mutant NLRP3 variant with pyruvate, the end-product of glycolysis. Pyruvate was able to increase the release of IL-1β, but not of IL-18, in unprimed macrophages expressing the p.D303N NLRP3 variant (**Figure 10A**). Pyruvate did not affected IL-1β release when the wild type NLRP3 was expressed in the macrophages (**Figure 10A**). In fact, when the p.D303N variant was expressed in macrophages, there was a subtle elevation in IL-1β gene expression, an effect not seen with the wild-type NLRP3 (**Figure 10B**). Contrarily, when glycolysis was impaired by blocking hexokinase activity with 2-deoxy-D-glucose (2DG) (**Supplementary Fig. 8E**), we observed a decrease in IL-1β release, but not in IL-18 (**Figure 10C**). As expected, 2DG also blocked IL-1β release upon canonical activation of the wild type NLRP3 (**Supplementary Fig. 8F**). In summary, our findings show that NLRP3 harbouring CAPS-associated pathogenic variants produces basal active inflammasomes even without cell priming. This spontaneous activation leads to the constitutive production of IL-18 and changes in the immunometabolism, marked by reduced glycolysis which in turn lessens

456 IL-1β production, limiting inflammatory flares but producing a positive basal protection
457 against pathogens.

DISCUSSION

Our study reveals that pathogenic variants in *NLRP3* associated with CAPS can constitutively activate NLRP3 inflammasomes even in the absence of triggers or priming signals. The expression level of this pathogenic NLRP3 variants directly associates with increased inflammasome activity (ASC oligomer formation, caspase-1 activation, GSDMD processing, IL-18 release and pyroptosis), as well as heightened basal inflammatory gene expression (i.e., upregulation of nuclear receptor 4A). We discovered that triggers activating NF-κB pathway enhance the activation of the inflammasome carrying pathogenic NLRP3 variants and broaden the range of molecules released from macrophages. A notable outcome is a significant induction of IL-1β release, a phenomenon scarcely observed upon constitutive activation of NLRP3 in unprimed cells, despite increased *IL1B* gene expression. This can be attributed to the altered immunometabolism observed during basal NLRP3 activation linked with CAPS-associated variants, which, among others, impairs glycolysis curbing IL-1β production and limiting pathogenic inflammatory flares, while preserving a basal inflammatory status as a defence mechanism against pathogens.

Most of the previously published research on the functional characterization of mutant NLRP3 variants has been conducted by exposing monocytes or macrophages to LPS for a span of 2 to 5 hours, followed by measuring the release of IL-1β [i.e. [6,12]]. Under these experimental conditions, the release of IL-1β is exacerbated by LPS in samples from CAPS patients compared to those carrying wild type NLRP3, while it is usually undetectable in unprimed cells. A detailed analysis of additional aspects of NLRP3 inflammasome activation reveal that in basal unprimed cells there is no observation of caspase-1 activation, IL-18 release, processing of GSDMD or pyroptosis [10–16]. These considerations differ from the results of our study. The discrepancies may be due to the brief culture period of the unprimed cells in previous studies, which likely causes only a minimal activation of the NLRP3 inflammasome making it challenging to detect.

Supporting this concept, our findings indicate that a low *NLRP3* expression, induced by a 2 hour doxycycline incubation, was insufficient to trigger detectable GSDMD cleavage or IL-18 release by using our methods. Given that *NLRP3* and *IL1B* gene expression in myeloid cells is strongly induced following NF-κB activation [18,32], LPS priming is expected to enhance *NLRP3* expression in cells from CAPS patients, yet mutant NLRP3 can constitutively assemble active inflammasomes. Although NLRP3 expression in CAPS patients with active diseases is comparable to that of healthy donors, as per GEO datasets (GSE57253)[30], LPS has been commonly used in previous studies to stimulate IL-1β expression and release from CAPS samples [10–16]. Our recombinant system, which uses NLRP3-deficient immortalized macrophages, effectively mirrors the monocyte behavior seen in CAPS patients and their IL-1β release upon LPS exposure. By adjusting doxycycline levels or incubation durations we controlled mutant NLRP3 gene expression and we discovered that, even without priming signals, there was a constitutive functional activation of the inflammasome reliant on *NLRP3* gene expression. Consequently, the measurement of IL-1β release in CAPS-related cells should not be the only marker of inflammasome activation in the absence of NF-κB induction. Our study demonstrates that macrophages carrying pathogenic NLRP3 variants trigger IL-1β release when treated with various NF-κB activators, including TLR2 agonist Pam3-CSK_4. Most importantly, several host-related compounds like palmitate, S100A9 or IL-6 also elicit this response. Interestingly, responses varied among the different NLRP3 mutations we studied; the p.T348M mutation, in particular, resulted in reduced IL-1β release. These findings broaden the range of molecules known to trigger a robust IL-1β–driven response in both active CAPS patients beyond just LPS. Notably, S100A9 and IL-6 levels have been previously reported to be elevated in both CAPS patients and animal models of the disease [30,33–36]. However, the lack of the IL-6 receptor in the murine model does not alter the pathology [37], thus suggesting that while recombinant IL-6 could induce IL-1β release in our immortalized macrophage system, it may not be directly linked to CAPS

pathophysiology [37]. This is further supported by the inability of IL-6 to prompt IL-1β release in blood samples from CAPS patients.

The conclusions of our study are reinforced by previous research that identified activation of the NLRP3 in unprimed primary PBMCs from CAPS patients and in recombinant THP-1 cells expressing mutant NLRP3 [38–41]. Other studies have also highlighted increased reactive oxygen species production, ATP release and reduced cell survival in unstimulated monocytes from CAPS patients [42–44]. Our research further emphasizes the inherent activity of the NLRP3 inflammasome associated with CAPS. We also found that pathogenic NLRP3 variants exhibiting basal inflammasome activation are modulated by ubiquitination, a known inhibitor of the canonical NLRP3 inflammasome activation [17]. This is consistent with recent insights indicating that pharmacological targeting of NLRP3 deubiquitination inhibits the activation of multiple pathogenic NLRP3 variants [45]. Moreover, other post-transcriptional NLRP3 modifications, like phosphorylation, have been proposed to modulate the gain-of-function behaviour of pathogenic NLRP3 variants [46]. Thus, managing post-transcriptional NLRP3 priming at various levels, such as blocking NF-κB activation to downregulate the *NLRP3* gene expression, might offer avenues to treat or prevent inflammatory outbreaks in CAPS patients [40].

While our research uncovered various triggers, including endogenous ones, that modulate the activity of the mutant NLRP3 inflammasome, CAPS are classified as autoinflammatory syndromes [47]. Our data supports this classification, and suggest that it could be due to the expression of a constitutively active NLRP3 inflammasome. Consistently, the systemic expression of NLRP3 with gain-of-function pathogenic variants in a murine CAPS model replicates a sterile inflammation phenotype even without any trigger. These clinical manifestations range from animal growth impediments, sterile skin abscesses, hair loss, arthropathy and osteoporosis, to splenomegaly, lymphopenia, liver fibrosis, saccular-stage lung morphogenesis and peritonitis, all leading to premature death [13,15,35–37,44,48–50]. The inflammatory disease in these animals is driven by various mechanisms, including the ASC/caspase-1

inflammasome, cytokines IL-1β, IL-18, TNF-α and GSDMD-mediated pyroptosis [35,48,50]. Nonetheless, we identified additional secretome regulated by pathogenic NLRP3 variants that could also contribute to the perpetuation of inflammatory flares in CAPS patients. This includes the release of IL-1α, HMGB1 or the purinergic P2X7 receptor. Interestingly, the plasma concentration of P2X7 receptor has been found to increase in patients during different inflammatory pathologies and correlates positively with the plasma concentration of C-reactive protein [51–54]. Our results suggest that the plasma concentration of P2X7 receptor might also serve as a potential biomarker for CAPS-related inflammation, akin to C-reactive protein [55].

Additionally, the constitutive activation of NLRP3 inflammasomes carrying pathogenic variants dictates a gene expression program that increases inflammatory genes. This includes the upregulation of nuclear receptors 4A1 and 4A2, which although not previously associated with CAPS, control the inflammatory activation of macrophages and have been implicated in rheumatic diseases [56]. CAPS-associated NLRP3 variants also control other genes related to innate immunity (such as lipocalin 2, C-C chemokine receptor type 7, or the zinc finger endoribonuclease Zc3h12a) and IL-17 responses. This is significant since cutaneous manifestations of CAPS are driven by IL-17 [13]. Furthermore, the expression of pathogenic NLRP3 variants was associated with upregulated defence mechanisms against viruses, which may explain the clinical observation that untreated CAPS patients are not prone to suffer from infections. Conversely, cellular homeostatic processes were downregulated upon expression of CAPS-associated NLRP3 variants.

Advances in the field of immunometabolism have revealed how metabolic processes are crucial to regulate the inflammatory function of macrophages, with impact on the progress of diseases [28,29]. Stimulation of macrophages with LPS triggers metabolic reprogramming, leading to enhanced glycolysis and an upregulated pentose phosphate pathway, while reducing the tricarboxylic acid cycle [28]. Our study determined that the basal activation of the CAPS-associated NLRP3 inflammasome significantly alters

cellular metabolites, including lipids, lipids-like molecules, amino acids and their intermediates. These findings are further supported by the upregulation of biological processes and genes associated with these pathways. Interestingly, echoing the metabolic transition from oxidative metabolism to glycolysis seen post-LPS stimulation in macrophages [28,29], we found that certain key glycolytic genes (such as *PFKFB3* or *BPGM*) were upregulated in blood cells from CAPS patients collected during active disease, while others (*ENO3*) were downregulated. On a cellular level, the basal activation of the CAPS–associated NLRP3 inflammasome resulted in decreased expression of glycolytic genes and a reduction in glycolysis flux and glycolytic ATP production. This led to a specific limitation of IL-1β production, potentially impairing IL-1–driven inflammatory flares, while maintaining IL-18 release and a basal innate immune activation in CAPS, which is crucial for protection against pathogens. Beyond the downregulation of glycolytic genes, it is known that caspase-1 activation can also reduce glycolysis by processing key glycolytic enzymes [57].

One limitation of this study is the potential discrepancy between the gene expression and metabolic programs between immortalized mouse macrophages expressing the p.D303N NLRP3 variant and those from primary mouse macrophages or human monocytes/macrophages, both *in vitro* and *in vivo*. Furthermore, our study solely focused on the metabolism affected by one pathogenic NLRP3 variant (p.D303N) expressed in immortalized macrophages. Despite this, we observed that the metabolic profile and gene expression in monocytes from human CAPS patients carrying additional pathogenic NLRP3 variants were similar to those in immortalized macrophages expressing the p.D303N human NLRP3 variant. This observation suggests that a reduction in glycolysis could limit IL-1β–derived inflammatory flares in CAPS.

Overall, our study reveals that gain-of-function pathogenic NLRP3 variants, which are associated with CAPS, lead to the formation of a constitutively active inflammasome dependent on NLRP3 expression. This activation occurs even in the absence of triggers or cell priming, and it influences the immunometabolism of CAPS patients, specifically

596 by hindering glycolysis and consequently limiting IL-1β production and inflammatory
597 flares, but orchestrating a specific inflammatory programme against pathogens. Active
598 pathogenic inflammasomes can be further modulated by deubiquitination and signals
599 associated with pathogens or sterile triggers that activate the NF-κB pathway,
600 intensifying inflammasome-related responses, including IL-1β production and CAPS
601 flares.

METHODS

This research complies with all relevant ethical regulations, and the study protocol was approved by the ethical committee of the University Clinical Hospital Virgen de la Arrixaca (Murcia, Spain).

Reagents and buffers. Different reagents and their sources used in this study were: ATP, nigericin, BSA fatty acid-free and low endotoxin, palmitic acid, doxycycline, MCC950 (CP-456773), and the authentic standards citric acid, malic acid, fumaric acid, succinic acid, ketoglutaric acid, pyruvic acid and lactic acid were all purchased from Sigma-Aldrich; Palmitic acid was conjugated with BSA as described previously [58]; ultrapure *E. coli* LPS serotype 0111:B4 (tlrl-3pelps) and Pam3CSK$_4$ (tlrl-pms) from InvivoGen; recombinant mouse IL-1Ra protein (HY-P72566) from MedChemExpress; recombinant mouse IL-6 protein (RMIL6I) from Invitrogen; recombinant mouse S100A9 protein (2065-s9), recombinant human S100A9 protein (9254-s9), recombinant human IL-6 protein (7270-IL/CF) from R&D systems; Pyruvate (L064-100) from Biowest; 2-deoxy-D-glucose (2-DG) (14325), ubiquitin isopeptidase inhibitor I G5 (21006), PR619 (16276) and b-AP15 (11324) from Cayman Chemical Company. Acetonitrile and water 0.1% (v/v) formic acid were from J,T. Baker, and formic acid was obtained from Panreac. Ultrapure water filter through Milli-Q system (Millipore Corp).

Human samples. Samples and data from humans volunteers included in this study, who gave written informed consent, were stored in the Biobanco en Red de la Región de Murcia, BIOBANC-MUR, registered on the National Registry of Biobanks with registration number B.0000859, and were used following standard operating procedures with appropriate approval of the Ethical Committee of the Clinical University Hospital Virgen de la Arrixaca (Murcia, Spain). Gender was not considered in this study, as CAPS is a rare condition and scare patients are available to equilibrate among genders (**Supplementary Table 1**). Whole blood samples were collected in EDTA anticoagulated

tubes from healthy donors (*n*= 9) and from individuals with CAPS (MWS) carrying the NLRP3 p.R260W (*n*= 1), p.D303N (*n*= 1), p.T348M (*n*= 1) and p.A439T variant (*n*= 4). Samples were all used to obtain the results of this study. CAPS patients were with inactive disease under IL-1 blocking therapy by the time blood was extracted (**Supplementary Table 1**). Human peripheral blood mononuclear cells (PBMCs) were isolated using Ficoll Histopaque-1077 (Sigma-Aldrich) and cultured in Opti-MEM Reduced Serum Media (Gibco) at 37ºC and 5% CO_2. Cells were stimulated with LPS (100 ng/ml), Pam3-CSK_4 (1 µg/ml), recombinant human S100A9 protein (500 ng/ml), recombinant human IL-6 protein (500 ng/ml), palmitate-BSA conjugated (1 mM) and MCC950 (10 µM) during 2, 4 and 6 hours in Opti-MEM. In some experiments, cells were treated with G5 and b-AP15 (both at 5 µM) in absence or presence of LPS for 6 hours.

Monocyte purification. Monocytes were isolated from PBMCs using the MagniSort™ Human CD14 Positive Selection Kit (Thermofisher) and $2x10^6$ monocytes were cultured in Opti-MEM Reduced Serum Media (Life Technologies) at 37ºC and 5% CO_2 in presence or absence of 500 ng/ml LPS for 2 hours. Control cultures without cells were run in parallel as metabolic control.

Immortalized mouse macrophages generation and stimulation. For doxycycline-inducible expression of NLRP3 variants in *Nlrp3*$^{-/-}$ immortalized mouse macrophages (a gift from I. Hafner-Bratkovič, National Institute of Chemistry, Ljubljana, Slovenia), we used the Tet-ON retroviral system (Clontech) with NLRP3-YFP wild type or p.D303N, p.T348M and p.R260W mutants [22,25]. Cells were treated with doxycycline (0.25, 0.5 and 1 µg/ml) to express NLRP3, in the presence or absence of MCC950, ATP, MSU, LPS, Pam3-CSK_4, S100A9, IL-6, or palmitate at different concentrations and incubation times as indicated in the figure legends. In some experiments, the cells were also incubated with pyruvate (10 mM), the following deubiquitinase inhibitors G5 (5 µM), PR-619 (10 µM) and b-AP15 (5 µM), or with the glycolysis inhibitor 2-DG (0.1, 0.5 or 1 mM).

Ultra-performance liquid-chromatography-electrospray ionization-quadrupole time-of-flight mass-spectrometry (UPLC-ESI-QTOF-MS) untargeted metabolomics analysis. After stimulation, cells were washed with PBS twice and resuspended in 2 ml (monocytes) or 800 μl (macrophages) of MeOH (PanReac AppliChem) to obtain polar metabolites. Four replicates of each group were processed. Samples were homogenised in a vortex for 1 min, and then centrifuged for 10 min at 6,000 xg at 4°C (Thermo Scientific). The resultant supernatants were filtered through a 0.22 µm PVDF filter prior the injection in the UPLC-ESI-QTOF-MS system. Four replicates each one from an individual donor of each group were processed in monocytes. The analyses were performed by an Agilent 1290 Infinity LC system coupled to a 6550 Accurate-Mass Quadrupole time-of-flight (QTOF) (Agilent Technologies) using an electrospray interface (Jet Stream Technology). Chromatographic separation was carried out on a reversed-phase C18 column (Poroshell 120, 3 × 100 mm, 2.7 µm pore size) at 30 °C, using water with 0.1% formic acid (Phase A) and acetonitrile with 0.1% formic acid (Phase B) as mobile phases with a flow rate of 0.4 ml/min. The following gradient was used: 0–10 min, 1–18% phase-B; 10–16 min, 18–38% phase-B; 16–22 min, 38–95% phase-B. Finally, the phase B content was returned to the initial conditions (1%) for 1 min and the column re-equilibrated then for 5 min. The mass analyser was operated in negative mode under the following conditions: gas temperature 180 ºC, drying gas 12 l/min, nebulizer pressure 45 psig, sheath gas temperature 350 ºC, sheath gas flow 11 l/min, capillary voltage 3500 V, nozzle voltage 250 V, fragmentor voltage 350 V, and octapole radiofrequency voltage 250 V. Data were acquired over the *m/z* range of 50–1700 at the rate of 2 spectra/s. The data were acquired in negative and positive polarities. The raw data files were acquired by the UPLC-ESI-QTOF-MS system in profile file mode and were exported to MZmine software (Version 2.53, © 2005-2015 MZmine Development Team) to create the data matrix. The raw data generated of both polarities were pre-processed separately by a batch set of parameters including the mass detection, chromatogram builder and

deconvolution and alignment algorithm. The data matrices were then merged by MZmine and exported to Mass Profiler professional (MPP, Agilent technologies) and Metaboanalyst 5.0 online platform (www.metaboanalyst.ca) for parallel data management. Data matrices were processed including log transformation and auto scaling prior to univariate and multivariate analysis [59]. The multivariate analysis PCA (Principal component analysis) was performed to study the total data variation of the data samples groups and evaluate the group trends. The calculated PCA model was built based on 16 samples and three components in monocytes, or 12 samples and three components in macrophages. The first two principal components PC1 and PC2 explained 25.2% and 9.6% of the total variability for monocytes, and 29.5% and 15.9% of the total variability in case of macrophages. Both PCA models showed the differences according to the total covariance between the study groups. The univariate analysis was performed by MPP software after the multivariate analysis evaluation. Data treatment through MPP software included filters by frequency of the data matrix to reduce the sample variability within each study group. ANOVA and *t*-test unpaired (corrected *p*-value cut-off: 0.05; *p*-value computation: asymptotic; multiple testing correction: Benjamini-Hochberg) statistics analysis was applied to the data matrix to filter significant entities along the different sample groups. The final list of features was used for metabolite identification with databases according to the exact mass and therefore achieving level 2 of identification [60]. Metabolomic data obtained in this study has been deposited in MetaboLights under the accession code MTBLS7872 [https://www.ebi.ac.uk/metabolights/MTBLS7872].

UPLC-ESI-QTOF-MS targeted metabolomics analysis of glycolysis and TCA cycle. The analyses were set up according to Körver-Keularts et al [61] with modifications. The UPLC-ESI-QTOF-MS system used for the targeted approach was the same as for untargeted except the reversed-phase column. Chromatographic separation was carried out on a Acquity C18 column UPLC HSS T3 1.8 µm 2.1 × 100 mm at 22 °C, using water

with 0.1% formic acid (Phase A) and 95% acetonitrile/1% water with 0.1% formic acid (Phase B) as mobile phases with a flow rate of 0.45 ml/min. The following gradient was used: 0–2 min, 0% phase-B; 2–4 min, 0–15% phase-B; 4–10 min, 15–45% phase-B; 10–13 min, 45–100% phase-B; 13–20 min, 100% phase-B; 20–25 min, 0% phase-B; 25–35 min, phase-B. The mass analyser was operated in negative mode under the following conditions: gas temperature 150 ºC, drying gas 15 l/min, nebulizer pressure 35 psig, sheath gas temperature 400 ºC, sheath gas flow 12 l/min, capillary voltage 3500 V, nozzle voltage 500 V, fragmentor voltage 100 V, and octapole radiofrequency voltage 750 V. Data were acquired over the *m/z* range of 50–1200 at the rate of 3.5 spectra/s. The data were acquired in negative mode. The raw data files were acquired by the UPLC-ESI-QTOF-MS system in profile file mode and were exported to MassHunter Qualitative Analysis software (Version 10.0, Agilent Technologies) for metabolite identification.

Transcriptome and gene expression analysis. Data from RNA sequencing from total blood cells from healthy pediatric donors (*n*= 5), pediatrics CAPS patients carrying the NLRP3 p.G569R variant with active disease (NOMID/CINCA) prior to anakinra treatment (*n*= 7), and the same CAPS patients with inactive disease following anakinra treatment (GSE57253) [https://www.ncbi.nlm.nih.gov/geo/query/acc.cgi?acc=GSE57253] [30] were analyzed with the package DESeq2 (R studio, Posit, PBC) to calculate differential inflammatory and metabolic gene expression. Data from healthy human PBMCs (*n*= 26-30) *in vitro* treated or not during 4 h with LPS (10 ng/ml) (GSE42606) [https://www.ncbi.nlm.nih.gov/geo/query/acc.cgi?acc=GSE42606] [62] was analyzed with the GEO2R tool with the package Limma (R studio, Posit, PBC) to calculate differential inflammatory and metabolic gene expression. Data from total blood cells from healthy donors (*n*= 6) and CAPS patients with active disease (*n*=3) (GSE17732) [https://www.ncbi.nlm.nih.gov/geo/query/acc.cgi?acc=GSE17732] [31] was analyzed with the GEO2R tool with the package Limma (R studio, Posit, PBC) to calculate differential metabolic gene expression.

Total RNA was extracted from *Nlrp3*$^{-/-}$ immortalized mouse macrophages expressing NLRP3 wild type or NLRP3 p.D303N using the RNeasy kit (74104, Qiagen) following manufacturer instructions. Upon extraction, total RNA was quantified with Qubit RNA BR Assay (Invitrogen), and RNA integrity was analysed with TapeStation 4200 (Agilent Technologies). All samples showed RIN >8. cDNA synthesis and library generation were performed using Stranded mRNA Prep Kit (Illumina) following the manufacturer's instructions. RNA-seq libraries were sequenced using Paired-End 200 bases (PE200) sequencing chemistry on NextSeq 2000 Sequencing Systems (Illumina). Sequencing results were analysed using package DESeq2 (R studio, Posit, PBC) for differential analysis of gene expression between two groups. Data generated in this study has been deposited in GEO under accession code GSE246713 [https://www.ncbi.nlm.nih.gov/geo/query/acc.cgi?acc=GSE246713]. In this case, the Wald test was used, and data were corrected with the Benjamini-Hochberg procedure to obtain an adjusted *p*-value. For group representation, all data were normalized using vst DESeq2 function. Enrichment analysis of gene ontology (GO) was determined using the DAVID tool v2021[63,64], the Benjamini–Hochberg method are used to correct the *p*-values, gene sets with adjusted *p*-value < 0.05 were significantly enriched.

HEK293T cell culture and transfection. HEK293T cells (CRL-11268, American Type Culture Collection) were maintained in Dulbecco's modified Eagle's medium (DMEM)/ F-12 (1:1) (Lonza) supplemented with 10% foetal calf serum (FCS) (Life Technologies), 2 mM GlutaMAX (Life Technologies), and 1% penicillin-streptomycin (Life Technologies). Cells were maintained at 37 ºC in a humidified 5% CO_2 incubator. Lipofectamine 2000 (Life Technologies) was used for the transfection of $7x10^5$ HEK293T according to the manufacturer's instructions using 0.1 µg of ASC-RFP plasmid and 0.1 µg of YFP-NLRP3-Luc plasmid and/or YFP-NLRP3 D303N-Luc plasmid [22,55].

Flow cytometry. Intracellular ASC-speck formation in human monocytes was evaluated by seeding 50 µl of individuals' whole blood samples in polystyrene flow cytometry tubes (Falcon) with RPMI 1640 medium (Lonza) containing 10% FCS and 2mM Glutamax. Following treatments with inhibitor or triggers, cells were stained for the detection of ASC specks by Time-of-Flight Inflammasome Evaluation (TOFIE) [65,66] using the PE conjugated mouse monoclonal anti-ASC antibody (clone HASC-71, catalogue 653903, Biolegend, 1:500). Monocytes were gated using the FITC conjugated mouse monoclonal anti-CD14 antibody (clone M5E2, catalogue 557153, BD Biosciences, 1:10) and using the PE-Cy7 conjugated mouse monoclonal anti-CD16 antibody (clone 3G8, catalogue 557744, BD Biosciences 1:10). Intracellular ASC-RFP-speck formation in HEK293T cells was evaluated after 24 h post-transfection by TOFIE in different gates with increasing mean fluorescence intensity for NLRP3-YFP (**Supplementary Fig. 2D**). Human blood samples were analysed by flow cytometry using FACS Canto (BD Biosciences) and for HEK293T cells using LSRFortessa (BD Biosciences), for both cases the FCS express software (De Novo Software) was used.

Fluorescence microscopy. Poly-L-lysine coated coverslips (Corning) were used to seed cells immortalized mouse macrophages *Nlrp3*$^{-/-}$ expressing the different variants of NLRP3. Cells were washed after stimulation once with sterile PBS buffer (Gibco) and fixed for 15 min at room temperature with 4% paraformaldehyde (Electron Microscopy Science) and then were washed four times with PBS. Cells were blocked with 0.5% bovine serum albumin (Sigma-Aldrich) and permeabilized with 0.1% Triton X-100 (Sigma-Aldrich) for 40 min at room temperature. Then, cells were incubated for 16 h at 4ºC with the primary rabbit polyclonal antibody anti-ASC (N-15)-R (catalogue sc-22514-R, Santa Cruz, 1:500). Cells were washed tree times for 10 min each and then incubated for 1 h with donkey anti-rabbit alexa-647 antibody (catalogue A31573, Life Technologies, 1:800). Then cells were washed three times for 10 min each and nuclei were stained with DAPI (1:10,000) for 10 min and coverslips were mounted on slides with mounting

797 medium (Dako). Images were acquired with a Nikon Eclipse *Ti* microscope equipped
798 with a 20× S Plan Fluor objective (numerical aperture, 0.45) and a digital Sight DS-QiMc
799 camera (Nikon) and 387 nm/447 nm, 543 nm/593 nm filter sets (Semrock), and the NIS-
800 Elements AR software (Nikon). Images were analysed with ImageJ (US National
801 Institutes of Health). Quantification of ASC specking macrophages was done in 4 fields
802 of view per condition and at least from *n*= 3 different experiments, counting at least a
803 total of 1,100 cells per condition.
804
805 **Western blot.** Immortalized mouse macrophages and HEK293T were lysed after
806 stimulation in ice-cold lysis buffer (50 mM Tris-HCl pH 8.0, 150 mM NaCl, 2% Triton X-
807 100) supplemented with 100 µl/ml of protease inhibitor mixture (Sigma-Aldrich) for 30
808 min on ice and were then centrifugated at 13,000 x*g* for 10 min at 4 °C. Cells lysates
809 were quantified by Bradford assay (Sigma-Aldrich) and results were read in a Synergy
810 Mx (BioTek) plate reader at 595 nm. Cell supernatants were collected, centrifuged at 600
811 x*g* for 5 min at 4 °C and the cell-free supernatants were concentrated using a 10 kDa
812 cut-off column (UFC501024, Merk-Millipore). Cells lysates and concentrated
813 supernatants were denaturalized with Laemmli buffer (Sigma-Aldrich) and heated at
814 95ºC for 5 min. 40 µg of cell lysates or from 0.5 to 1 ml of concentrated supernatants
815 were resolved in a 12% precast Criterion polyacrylamide gels (Biorad) and transferred
816 to nitrocellulose membranes (Biorad) by electroblotting. Membranes were hybridized
817 with the following primary antibodies: anti-NLRP3 mouse monoclonal (Cryo-2 clone,
818 catalogue AG-20B-0014, Adipogen, 1:1000), anti-Caspase 1 (p20) mouse monoclonal
819 (Casper-1, catalogue AG-20B-0042, Adipogen, 1:1000), anti-GSDMD rabbit monoclonal
820 (EPR19828, catalogue ab209845, Abcam, 1:2500), anti-IL-1β rabbit polyclonal (H-153;
821 catalogue sc-7884, 1:1000) and horseradish peroxidase (HRP)-anti-β-actin (C4;
822 catalogue sc-47778HRP, Santa Cruz, 1:10,000) and appropriate secondary antibodies:
823 horseradish peroxidase anti-IgG rabbit (catalogue NA9340V, Cytiva, 1:5,000) and
824 horseradish peroxidase anti-IgG mouse (catalogue NA9341V, Cytiva, 1:5,000).

Membranes were revealed using ECL Plus reagents (Cytiva) in a ChemiDoc Imaging System (BioRad).

Seahorse assay. *Nlrp3*$^{-/-}$ immortalized macrophages expressing or not NLRP3 p.D303N variant and NLRP3 wild type were seeded at 25.000 cells/well in Seahorse adherent 96-well plate (Agilent Technologies) in DMEM high glucose medium (Biowest) without FBS. Cells were treated with doxycycline (1 µg/ml), LPS (100 ng/ml), MCC950 (10 µM), IL-1Ra (100 ng/ml) or 2-DG (0.1, 0.5, 1 mM) for 4h or 16h (as indicated in the figure legend) at 37ºC and 5% CO_2. After stimulation, cell media was discarded, and the cells were incubated with 180 µl DMEM seahorse medium supplemented with 5 mM glucose, 1 mM pyruvate and 2 mM glutamine (Agilent Technologies). The plate was incubated for 45 min at 37°C without CO_2. Glycolytic rate assay, ATP real-time rate assay, and Cell Mito-stress kits (Agilent Technologies) were used for experiments according to the manufacturer's instructions using an XF96e Analyzer (Agilent Technologies). After reading, the nuclei of the cells were stained with 3 mM Hoechst solution (Sigma-Aldrich) to normalize the number of cells in the calculated OCR and ECAR values. Results were collected with the Wave software version 2.6 (Agilent Technologies).

L-Lactate determination. To measure glycolysis, the presence of L-lactate in cell-free supernatants was measured using the Glycolysis assay kit (BA0086, Assay Genie) according to the manufacturer's instructions, the samples were read in a Synergy Mx plate reader (BioTek) at 565 nm.

Lactate dehydrogenase assay. To measure cell death, the LDH present in cell-free supernatants was detected using the Cytotoxicity Detection kit (Roche) according to manufacturer instructions, the reaction was read in a Synergy Mx (BioTek) plate reader at 492 nm and corrected at 620 nm.

NF-κB reporter assay. To evaluate NF-κB activation we used the RAW264.7 macrophage cell line expressing a secreted embryonic alkaline phosphatase (SEAP) reporter gen under the control of the NF-κB promoter (Invivogen), which were cultured according to manufacturer instructions. Cells were treated with ATP (5 mM), MSU (200 µg/ml), LPS (100 ng/ml), Pam3-CSK_4 (1 µg/ml), S100A9 (500 ng/ml), IL-6 (500 ng/ml), and palmitate (1 mM) for 4 hours, in the presence or absence of G5 (5 µM), PR-619 (10 µM) and b-AP15 (5 µM). Or with LPS with G5, PR-619 and b-AP15 for 6 hours. Cell supernatants were collected, centrifuged at 600 x*g* for 5 min at 4 °C and the cell-free supernatants were mixed with the Quanti-blue solution (rep-qbs, Invivogen) according to manufacturer instructions. The reaction was read in a Synergy Mx (BioTek) plate reader at 622 nm.

ELISA. Cell-free supernatants were collected and the following ELISA kits were used according to manufacturer instructions: mouse IL-1β (88-7013-22, Invitrogen), mouse TNF-α (88-7324-22, Invitrogen), mouse IL-18 (BMS618-3, Invitrogen), mouse P2X7 (OKEH05605, Aviva Systems Biology), mouse Cathepsin B (ab119585, Abcam), mouse Annexin A1 (ab264613, Abcam), mouse IL-1α (MLA00, R&D Systems), mouse HMGB1 (ARG81310, Arigo), mouse CD14 (D4982, R&D Systems), mouse Cystatin B (Cstb, orb565550, Biorbyt), mouse CD206 (orb546630, Biorbyt), human IL-18 (7620, MBL), human galectina 3 (BMS279-4, Invitrogen), human IL-1β (BMS224INST, Invitrogen) and human TNF-α (DTA00D, R&D Systems). ELISA were read in a Synergy Mx (BioTek) plate reader at 450 nm and corrected at 540 and 620 nm.

Quantitative reverse transcriptase-PCR analysis. Total RNA was extracted and purified from immortalized macrophages using the RNeasy kit (74104, Qiagen) following manufacturer instructions and quantified in a NanoDrop 2000 (Thermo Fisher). RNA was reverse transcripted using the iScript™ cDNA Synthesis kit (1708891, BioRad) according

881 to manufacturer instructions. Quantitative PCR was done in an iQTM 5 Real Time PCR
882 System (BioRad) with SYBR Green mix (Takara) and predesigned KiCqStart primers for
883 mouse *Il1b, Tnfa, Il18, Pycard, Gsdmd, Nlrp3, Nek7* and *Casp1* (Sigma-Aldrich). Gene
884 expression was normalized with *Gapdh* as endogenous control.
885
886 **Statistics and reproducibility.** Statistical analyses were performed using GraphPad
887 Prism 9 (GraphPad Software Inc) or R-Studio (Posit, PBC). Normality of the samples
888 was determined with D'Angostino and Pearson omnibus K2 normality test. Outliers from
889 data sets were identified by the ROUT method with *Q*= 1% and were eliminated from the
890 analysis and representation. All data are shown as mean values and errors bars
891 represent standard error (SEM). For two-group comparisons, the Mann-Whitney U test
892 was used in non-parametric data, and the *t*-test was used in parametric data. The
893 comparisons of multiple groups were analysed by Kruskal-Wallis for non-parametric data
894 and ANOVA analyses were used for parametric data. For dataset GSE42606 and
895 GSE17732, gene expression comparison was performed with *t*-test. For dataset
896 GSE57253 and immortalized mouse macrophages RNA sequencing the Wald test was
897 used. In all datasets, data were corrected with the Benjamini-Hochberg procedure to
898 obtain adjusted *p*-value. The *p* values are indicated with asterisks and ranges are noted
899 in the figure legends, for $p > 0.05$ was considered not significant (*ns*). The exact *n* number
900 of independent experiments for the figure 4 panels A and B were as follows:
901 For Figure 4A, for empty vector transduced macrophages *n*= 3 independent
902 experiments, except *n*= 4 independent experiments for untreated, LPS and palmitate; for
903 wild type NLRP3 transduced macrophages *n*= 3 independent experiments, except *n*= 4
904 independent experiments for untreated and LPS; for NLRP3 p.D303N transduced
905 macrophages *n*= 4 independent experiments, except *n*= 5 independent experiments for
906 untreated and LPS and *n*= 3 independent experiments for MCC950 treatments; for
907 NLRP3 p.R260W transduced macrophages *n*= 4 independent experiments, except *n*= 3
908 independent experiments for palmitate and S100A9; for NLRP3 p.T348M transduced

macrophages *n*= 5 independent experiments for untreated and LPS, *n*= 4 independent experiments for IL-6 and $Pam3CSK_4$, and *n*= 3 independent experiments for palmitate and S100A9 (each independent experiment is represented by a different symbol).

For Figure 4B, for empty vector transduced macrophages *n*= 3 independent experiments, except *n*= 4 independent experiments for untreated, LPS and palmitate; for wild type NLRP3 transduced macrophages *n*= 3 independent experiments, except *n*= 4 independent experiments for untreated and LPS; for NLRP3 p.D303N transduced macrophages *n*= 4 independent experiments for palmitate, S100A9 and IL-6, *n*= 5 independent experiments for untreated and LPS and *n*= 3 independent experiments for ATP, $Pam3CSK_4$, MSU and all MCC950 treatments; for NLRP3 p.R260W transduced macrophages *n*= 4 independent experiments, except *n*= 3 independent experiments for palmitate and S100A9; for NLRP3 p.T348M transduced macrophages *n*= 5 independent experiments, except *n*= 3 independent experiments for palmitate and S100A9 (each independent experiment is represented by a different symbol).

Inclusion and ethics. We support inclusive, diversity, and equilibrate conduct of research. Whenever possible, we worked to ensure gender balance, ethnic and other types of diversity in the recruitment of human subjects. The protocol to include samples and data from humans included in this study was approved by the Ethical Committee of the Clinical University Hospital Virgen de la Arrixaca (Murcia, Spain).

DATA AVAILABILITY

The metabolomic data generated in this study have been deposited in the MetaboLights database under accession code MTBLS7872 [https://www.ebi.ac.uk/metabolights/MTBLS7872]. The RNAseq data generated in this study have been deposited in the GEO database under accession code GSE246713 [https://www.ncbi.nlm.nih.gov/geo/query/acc.cgi?acc=GSE246713]. The RNAseq data used in this study are available in the GEO database under accession codes GSE57253, GSE42606 and GSE17732 [https://www.ncbi.nlm.nih.gov/geo/query/acc.cgi?acc=GSE57253; https://www.ncbi.nlm.nih.gov/geo/query/acc.cgi?acc=GSE42606; https://www.ncbi.nlm.nih.gov/geo/query/acc.cgi?acc=GSE17732]. Source data are provided with this paper.

REFERENCES

1. Coll, R. C., Schroder, K. & Pelegrín, P. NLRP3 and pyroptosis blockers for treating inflammatory diseases. *Trends Pharmacol Sci* (2022) doi:10.1016/j.tips.2022.04.003.

2. Broz, P., Pelegrín, P. & Shao, F. The gasdermins, a protein family executing cell death and inflammation. *Nat Rev Immunol* **20**, 143–157 (2020).

3. Gattorno, M. *et al.* Classification criteria for autoinflammatory recurrent fevers. *Ann Rheum Dis* **78**, 1025–1032 (2019).

4. de Torre-Minguela, C., Mesa del Castillo, P. & Pelegrín, P. The NLRP3 and Pyrin Inflammasomes: Implications in the Pathophysiology of Autoinflammatory Diseases. *Front Immunol* **8**, 43 (2017).

5. Booshehri, L. M. & Hoffman, H. M. CAPS and NLRP3. *J Clin Immunol* **39**, 277–286 (2019).

6. Mensa-Vilaro, A. *et al.* Late onset cryopyrin-associated periodic syndrome due to myeloid-restricted somatic NLRP3 mosaicism. *Arthritis Rheumatol* **68**, 3035–3041 (2016).

7. Tanaka, N. *et al.* High incidence of NLRP3 somatic mosaicism in patients with chronic infantile neurologic, cutaneous, articular syndrome: results of an International Multicenter Collaborative Study. *Arthritis Rheum* **63**, 3625–32 (2011).

8. Nakagawa, K. *et al.* Somatic NLRP3 mosaicism in Muckle-Wells syndrome. A genetic mechanism shared by different phenotypes of cryopyrin-associated periodic syndromes. *Ann Rheum Dis* **74**, 603–10 (2015).

9. Weber, A. N. R. *et al.* Effective ex vivo inhibition of Cryopyrin-Associated Periodic Syndrome (CAPS)-associated mutant NLRP3 inflammasome by MCC950/CRID3. *Rheumatology* (2022) doi:10.1093/rheumatology/keac273.

10. Vande Walle, L. *et al.* MCC950/CRID3 potently targets the NACHT domain of wildtype NLRP3 but not disease-associated mutants for inflammasome inhibition. *PLoS Biol* **17**, 1–24 (2019).

11. Duan, Y. *et al.* RACK1 Mediates NLRP3 Inflammasome Activation by Promoting NLRP3 Active Conformation and Inflammasome Assembly. *Cell Rep* **33**, 108405 (2020).

12. Agostini, L. *et al.* NALP3 forms an IL-1beta-processing inflammasome with increased activity in Muckle-Wells autoinflammatory disorder. *Immunity* **20**, 319–325 (2004).

13. Meng, G., Zhang, F., Fuss, I., Kitani, A. & Strober, W. A mutation in the Nlrp3 gene causing inflammasome hyperactivation potentiates Th17 cell-dominant immune responses. *Immunity* **30**, 860–874 (2009).

14. Coll, R. C. *et al.* A small-molecule inhibitor of the NLRP3 inflammasome for the treatment of inflammatory diseases. *Nat Med* **21**, 248–255 (2015).

15. Xiao, J. *et al.* Gasdermin D mediates the pathogenesis of neonatal-onset multisystem inflammatory disease in mice. *PLoS Biol* **16**, e3000047 (2018).

16. Semino, C., Carta, S., Gattorno, M., Sitia, R. & Rubartelli, A. Progressive waves of IL-1β release by primary human monocytes via sequential activation of vesicular and gasdermin D-mediated secretory pathways. *Cell Death Dis* **9**, 1088 (2018).

17. Juliana, C. *et al.* Non-Transcriptional Priming And Deubiquitination Regulate Nlrp3 Inflammasome Activation. *J Biol Chem* **287**, 36617–36622 (2012).

18. Bauernfeind, F. G. *et al.* Cutting edge: NF-kappaB activating pattern recognition and cytokine receptors license NLRP3 inflammasome activation by regulating NLRP3 expression. *J Immunol* **183**, 787–91 (2009).

19. Tapia-Abellán, A. *et al.* Sensing low intracellular potassium by NLRP3 results in a stable open structure that promotes inflammasome activation. *Sci Adv* **7**, eabf4468 (2021).

20. Hafner-Bratkovič, I. & Pelegrín, P. Ion homeostasis and ion channels in NLRP3 inflammasome activation and regulation. *Curr Opin Immunol* **52**, 8–17 (2018).

21. Li, W. *et al.* Engineered Pigs Carrying a Gain-of-Function NLRP3 Homozygous Mutation Can Survive to Adulthood and Accurately Recapitulate Human Systemic Spontaneous Inflammatory Responses. *J Immunol* **205**, 2532–2544 (2020).

22. Tapia-Abellán, A. *et al.* MCC950 closes the active conformation of NLRP3 to an inactive state. *Nat Chem Biol* **15**, 560–564 (2019).

23. Chen, J. & Chen, Z. J. PtdIns4P on dispersed trans-Golgi network mediates NLRP3 inflammasome activation. *Nature* **564**, 71–76 (2018).

24. Bujan-Rivas, S. *et al.* Novel evidences of atypical manifestations in cryopyrin-associated periodic syndromes. *Clin Exp Rheumatol* **35 Suppl 1**, 27–31 (2017).

25. Hafner-Bratkovič, I. *et al.* NLRP3 lacking the leucine-rich repeat domain can be fully activated via the canonical inflammasome pathway. *Nat Commun* **9**, 5182 (2018).

26. de Torre-Minguela, C., Barberà-Cremades, M., Gómez, A. I., Martín-Sánchez, F. & Pelegrín, P. Macrophage activation and polarization modify P2X7 receptor secretome influencing the inflammatory process. *Sci Rep* **6**, 22586 (2016).

27. Lopez-Castejon, G. Control of the inflammasome by the ubiquitin system. *FEBS J* **287**, 11–26 (2020).

28. Palsson-McDermott, E. M. *et al.* Pyruvate Kinase M2 Regulates Hif-1α Activity and IL-1β Induction and Is a Critical Determinant of the Warburg Effect in LPS-Activated Macrophages. *Cell Metab* **21**, 65–80 (2015).

29. O'Neill, L. A. J. & Pearce, E. J. Immunometabolism governs dendritic cell and macrophage function. *Journal of Experimental Medicine* vol. 213 15–23 Preprint at https://doi.org/10.1084/jem.20151570 (2016).

30. Canna, S. W. *et al.* An activating NLRC4 inflammasome mutation causes autoinflammation with recurrent macrophage activation syndrome. *Nat Genet* **46**, 1140–1146 (2014).

31. Stojanov, S. *et al.* Periodic fever, aphthous stomatitis, pharyngitis, and adenitis (PFAPA) is a disorder of innate immunity and Th1 activation responsive to IL-1 blockade. *Proc Natl Acad Sci U S A* **108**, 7148–53 (2011).

32. Dinarello, C. A. Interleukin-1beta and the autoinflammatory diseases. *N Engl J Med* **360**, 2467–2470 (2009).

33. Lachmann, H. J. *et al.* In vivo regulation of interleukin 1 in patients with cryopyrin-associated periodic syndromes. *Journal of Experimental Medicine* **206**, 1029–1036 (2009).

34. Aubert, P. *et al.* Homeostatic tissue responses in skin biopsies from NOMID patients with constitutive overproduction of IL-1β. *PLoS One* **7**, e49408 (2012).

35. Brydges, S. D. *et al.* Divergence of IL-1, IL-18, and cell death in NLRP3 inflammasomopathies. *J Clin Invest* **123**, 4695–705 (2013).

36. Brydges, S. D. *et al.* Inflammasome-mediated disease animal models reveal roles for innate but not adaptive immunity. *Immunity* **30**, 875–887 (2009).

37. McGeough, M. D. *et al.* Cutting edge: IL-6 is a marker of inflammation with no direct role in inflammasome-mediated mouse models. *J Immunol* **189**, 2707–11 (2012).

38. Kuemmerle-Deschner, J. B. *et al.* Clinical and Molecular Phenotypes of Low-Penetrance Variants of NLRP3: Diagnostic and Therapeutic Challenges. *Arthritis Rheumatol* **69**, 2233–2240 (2017).

39. Rieber, N. *et al.* A functional inflammasome activation assay differentiates patients with pathogenic NLRP3 mutations and symptomatic patients with low penetrance variants. *Clinical Immunology* **157**, 56–64 (2015).

40. Haverkamp, M. H., van de Vosse, E., Goldbach-Mansky, R. & Holland, S. M. Impaired cytokine responses in patients with cryopyrin-associated periodic syndrome (CAPS). *Clin Exp Immunol* **177**, 720–31 (2014).

41. Satoh, T., Kambe, N. & Matsue, H. NLRP3 activation induces ASC-dependent programmed necrotic cell death, which leads to neutrophilic inflammation. *Cell Death Dis* **4**, 1–8 (2013).

42. Tassi, S. *et al.* Altered redox state of monocytes from cryopyrin-associated periodic syndromes causes accelerated IL-1beta secretion. *Proc Natl Acad Sci U S A* **107**, 9789–94 (2010).

43. Carta, S. *et al.* Cell stress increases ATP release in NLRP3 inflammasome-mediated autoinflammatory diseases, resulting in cytokine imbalance. *Proceedings of the National Academy of Sciences* **112**, 2835–2840 (2015).

44. Bonar, S. L. *et al.* Constitutively activated NLRP3 inflammasome causes inflammation and abnormal skeletal development in mice. *PLoS One* **7**, e35979 (2012).

45. Ren, G.-M. *et al.* Pharmacological targeting of NLRP3 deubiquitination for treatment of NLRP3-associated inflammatory diseases. *Sci Immunol* **6**, (2021).

46. Song, N. *et al.* NLRP3 Phosphorylation Is an Essential Priming Event for Inflammasome Activation. *Mol Cell* **68**, 185-197.e6 (2017).

47. Gül, A. Dynamics of Inflammatory Response in Autoinflammatory Disorders: Autonomous and Hyperinflammatory States. *Front Immunol* **9**, 2422 (2018).

48. McGeough, M. D. *et al.* TNF regulates transcription of NLRP3 inflammasome components and inflammatory molecules in cryopyrinopathies. *Journal of Clinical Investigation* 1–10 (2017) doi:10.1172/JCI90699.

49. Wree, A. *et al.* NLRP3 inflammasome driven liver injury and fibrosis: Roles of IL-17 and TNF in mice. *Hepatology* **67**, 736–749 (2018).

50. Nakamura, Y. *et al.* Critical role for mast cells in interleukin-1beta-driven skin inflammation associated with an activating mutation in the nlrp3 protein. *Immunity* **37**, 85–95 (2012).

51. Giuliani, A. L. *et al.* The P2X7 Receptor Is Shed Into Circulation: Correlation With C-Reactive Protein Levels. *Front Immunol* **10**, 1–7 (2019).

52. Martínez-García, J. J. *et al.* P2X7 receptor induces mitochondrial failure in monocytes and compromises NLRP3 inflammasome activation during sepsis. *Nat Commun* **10**, 2711 (2019).

53. Conte, G. *et al.* Circulating P2X7 Receptor Signaling Components as Diagnostic Biomarkers for Temporal Lobe Epilepsy. *Cells* **10**, 2444 (2021).

54. García-Villalba, J. *et al.* Soluble P2X7 Receptor Is Elevated in the Plasma of COVID-19 Patients and Correlates With Disease Severity. *Front Immunol* **13**, 894470 (2022).

55. Baroja-Mazo, A. *et al.* The NLRP3 inflammasome is released as a particulate danger signal that amplifies the inflammatory response. *Nat Immunol* **15**, 738–748 (2014).

56. Murphy, E. P. & Crean, D. NR4A1-3 nuclear receptor activity and immune cell dysregulation in rheumatic diseases. *Front Med (Lausanne)* **9**, 874182 (2022).

57. Shao, W., Yeretssian, G., Doiron, K., Hussain, S. N. & Saleh, M. The Caspase-1 Digestome Identifies the Glycolysis Pathway as a Target during Infection and Septic Shock. *J Biol Chem* **282**, 36321–36329 (2007).

58. Peng, Z. *et al.* Nobiletin alleviates palmitic acid-induced NLRP3 inflammasome activation in a sirtuin 1-dependent manner in AML-12 cells. *Mol Med Rep* **18**, 5815–5822 (2018).

59. van den Berg, R. A., Hoefsloot, H. C. J., Westerhuis, J. A., Smilde, A. K. & van der Werf, M. J. Centering, scaling, and transformations: improving the biological information content of metabolomics data. *BMC Genomics* **7**, 142 (2006).

60. Sumner, L. W. *et al.* Proposed minimum reporting standards for chemical analysis Chemical Analysis Working Group (CAWG) Metabolomics Standards Initiative (MSI). *Metabolomics* **3**, 211–221 (2007).

61. Körver-Keularts, I. M. L. W. *et al.* Fast and accurate quantitative organic acid analysis with LC-QTOF/MS facilitates screening of patients for inborn errors of metabolism. *J Inherit Metab Dis* **41**, 415–424 (2018).

62. Smeekens, S. P. *et al.* Functional genomics identifies type I interferon pathway as central for host defense against Candida albicans. *Nat Commun* **4**, 1342 (2013).

63. Huang, D. W., Sherman, B. T. & Lempicki, R. A. Systematic and integrative analysis of large gene lists using DAVID bioinformatics resources. *Nat Protoc* **4**, 44–57 (2009).

64. Sherman, B. T. *et al.* DAVID: a web server for functional enrichment analysis and functional annotation of gene lists (2021 update). *Nucleic Acids Res* **50**, W216–W221 (2022).

65. Sester, D. P. *et al.* A Novel Flow Cytometric Method To Assess Inflammasome Formation. *The Journal of Immunology* **194**, 455–462 (2014).

66. Hurtado-Navarro, L., Baroja-Mazo, A., Martínez-Banaclocha, H. & Pelegrín, P. Assessment of ASC Oligomerization by Flow Cytometry. *Methods Mol Biol* **2459**, 1–9 (2022).

ACKNOWLEDGMENTS

We thank I. Hafner-Bratkovič (National Institute of Chemistry, Slovenia) for immortalized macrophages with Tet-ON system, M.C. Baños and A.I. Gomez (IMIB, Murcia, Spain) for technical assistance with molecular and cellular biology, Genomics central facility (IMIB, Murcia, Spain) for sequencing support, F. Perez-Sanz (Bioinformatics service, IMIB, Murcia, Spain) for RNA sequencing analysis, C. de Torre-Minguela (IMIB, Murcia, Spain) for initial help with metabolomics experiments design and the members of the Pelegrin's laboratory for comments and suggestions thought the development of this project. We are also particularly grateful for the generous contribution of the patients and the collaboration of Biobank Network of the Region of Murcia, BIOBANC-MUR. BIOBANC-MUR is supported by the "Instituto de Salud Carlos III (PT20/00109), by "Instituto Murciano de Investigación Biosanitaria Virgen de la Arrixaca, IMIB" and by "Consejería de Salud de la Comunidad Autónoma de la Región de Murcia. This work was supported by grants from MCIN/AEI/10.13039/501100011033 (grants PID2020-116709RB-I00, BG20/00060, CNS2022-135101 and RED2022-134511-T to PP), *FEDER/Ministerio de Ciencia, Innovación y Universidades – Agencia Estatal de Investigación* (grant SAF2017-88276-R to PP), Fundación Séneca (grants 20859/PI/18 and 21897/PI/22 to PP), the Instituto Salud Carlos III (grants DTS21/00080 and AC22/00009 to PP), the EU Horizon 2020 project PlasticHeal (grant 965196 to PP), the Spanish Ministry of Science, Innovation and Universities co-funded by the European Regional Development Fund / Agencia Estatal de Investigación (grant RTI2018-096824-B-C21 to JIA) and the Spanish Ministry of Science and Innovation / Agencia Estatal de Investigación (grant PID2021-125106OB-C31 to JIA). L.H-N. was supported by the fellowship 21214/FPI/19 (Fundación Séneca, Región de Murcia, Spain) and CM-L by was funded by the fellowship PRE2018-086824 (Ministerio economía y competitividad).

AUTHOR CONTRIBUTIONS STATEMENT

C.M-L. performed the experimental work; L.H-N. supported with human sample experimentation and performed flow cytometry experiments; D.A-B., A.T-A. supported with the generation of mutant NLRP3 and immortalized macrophage lines; J.R.M., C.V., S.B-R., J.I.A. obtained CAPS patient samples and clinical history; C.J.G., F.V. and F.A.T-B. performed and analyzed metabolomic assays; C.M-L. and P.P. analyzed the data, interpreted results, conceived the experiments, prepared the figures and paper writing; P.P. conceived the project, provided funding and overall supervision of this study.

COMPETING INTERESTS

P.P. declares that he is an inventor in a patent filled on March 2020 by the *Fundación para la Formación e Investigación Sanitaria de la Región de Murcia* (PCT/EP2020/056729) for a method to identify NLRP3-immunocompromised sepsis patients. P.P., L.H-N. and D.A-B. are co-founders and have shares in Viva in vitro diagnostics SL, but declare that the research was conducted in the absence of any commercial or financial relationships that could be construed as a potential conflict of interest. The remaining authors declare no competing interests.

FIGURE LEGENDS

Figure 1. Monocytes from CAPS patients show a constitutive inflammasome activation

(**A**) Percentage of ASC specking monocytes from healthy donors (HD, blue bars, *n*= 5 for 2h, *n*= 6 for 4h, *n*= 9 for 6h) and CAPS patients (grey bars, NLRP3 p.R260W, p.D303N, p.T348M and p.A439T, *n*= 5 for 2 and 6h, *n*= 7 for 4h) after whole blood treatment for different times with LPS (100 ng/ml).

(**B-E**) ELISA for galectin 3 (B), IL-18 (C), IL-1β (D) and TNF-α (E) release from PBMCs treated as indicated in panel A (*n*= 5 HD, *n*= 5 CAPS patients for 2h panels B,D,E, *n*= 7 CAPS patients for 2h panels B,D,E, *n*= 3 CAPS patients for panel C).

(**F-G**) Violin plot of *NLRP3*, *IL1B*, *TNFA*, *IL18* and *LGALS3* mRNA expression in PBMCs from healthy individuals treated or untreated with LPS (using dataset GSE42606) (F), or from blood cells of healthy individuals or CAPS patients with p.G569R NLRP3 mutation during an inflammatory flare without LPS treatment (using dataset GSE57253) (G). The median is indicated by the middle line.

Each dot corresponds to a different donor, and for CAPS, each colour represents a different mutation; data is represented as mean ± SEM; *t*-test two-sided was used to compare between the group of healthy donors and CAPS patients in panels A-E; *t*-test two-sided and Wald test two-sided, both with Benjamini–Hochberg correction, were used to compare gene expression in panels F,G; significance levels are indicated as follows: ***p < 0.0002; *ns* indicates no significant difference (p > 0.05). Source data are provided as a Source Data file.

Figure 2. Expression of CAPS-associated gain-of-function NLRP3 variants in macrophages results in constitutive active inflammasomes

(**A**) Western blot for NLRP3, GSDMD, and β-actin in cell lysates from *Nlrp3*$^{-/-}$ immortalized macrophages (iMos) treated for 16 h with or without doxycycline (0.25, 0.5

and 1 µg/ml) to induce the expression of the human wild type NLRP3 or p.D303N, p.R260W, and p.T348M variants in absence or presence of MCC950 (10 µM).

(**B**) Western blot for NLRP3, caspase-1, GSDMD and β-actin in cell lysates and supernatants from iMos expressing the human NLRP3 p.D303N treated as indicated in panel A with doxycycline at 1 µg/ml.

(**C**) Percentage of ASC specking iMos expressing the human wild type NLRP3 or p.D303N variant treated as indicated in panel A, but with the annotated doxycycline concentration to obtain a similar expression of both NLRP3.

(**D**) Percentage of extracellular LDH in iMos expressing human NLRP3 wild type or p.D303N variant treated as indicated in panel C.

(**E**) ELISA for IL-18 release from iMos treated as indicated in panel A.

Histograms in panels C-E present the mean ± SEM of *n*= 3 independent experiments (each one represented by a different symbol); Western blots are representative of *n*= 3 independent experiments; Ordinary one-way ANOVA test was used for panels C and E, *t*-test two-sided for panel D. Source data are provided as a Source Data file.

Figure 3. Increased expression of NLRP3 p.D303N results in higher inflammasome activation

(**A**) Western blot for NLRP3, GSDMD, and β-actin in cell lysates from *Nlrp3*$^{-/-}$ immortalized macrophages (iMos) treated for different times with or without 1 µg/ml doxycycline (2, 4, 8 or 16 h) to induce the expression of the human NLRP3 p.D303N, with or without LPS (100 ng/ml) and MCC950 (10 µM).

(**B,C**) Extracellular LDH (B) and ELISA for IL-18 release (C) from iMos treated as described in panel A, each independent experiment is represented by a different symbol in the histograms.

(**D**) Percentage of ASC specking HEK293T cells transfected with ASC-RFP and either NLRP3-YFP wild type (WT), the NLRP3 p.D303N-YFP variant, or a co-expression of

both NLRP3 WT and p.D303N-YFP. The expression levels of NLRP3 were determined by an increase in the mean fluorescence intensity.

(**E,F**) ELISA for IL-1β (E) and TNF-α (F) release from cells treated as indicated in panel A.

Western blots are representative of *n*= 2 independent experiments; Graphics are representative of *n*= 3 independent experiments (each one represented by a different symbol in the histograms) and data are represented as mean ± SEM; Two-way ANOVA test was used for panels B,C,E,F; for panel D *t*-test two-sided to compare p.D303N and the co-trasfection was used and Mann-Whitney U test two-sided was used when the wild type was compared to the co-trasfection or the p.D303N alone, significance levels are indicated as follows: *ns* indicates no significant difference ($p > 0.05$). For panel D, * indicates comparison with the wild-type NLRP3, and # indicates comparison within the p.D303N NLRP3 and the co-expression. Source data are provided as a Source Data file.

Figure 4. PAMPs and DAMPs are required to induce NF-κB–dependent IL-1β release from macrophages expressing pathogenic NLRP3 variants

(**A,B**) ELISA for IL-1β (A) and TNF-α (B) released from *Nlrp3*$^{-/-}$ immortalized macrophages (iMos) expressing the human wild type NLRP3 or the p.D303N, p.R260W, and p.T348M variants induced after 16 h treatment with doxycycline (1 µg/ml) and ATP (5 mM), MSU crystals (200 µg/ml), palmitate (1 mM), S100A9 (0.5 µg/ml), IL-6 (0.5 µg/ml), LPS (100 ng/ml) or Pam3-CSK_4 (1 µg/ml), together with or without MCC950 (10 µM).

(**C**) Colorimetric quantification of the levels of secreted alkaline phosphatase (SEAP) from NF-κB reporter RAW 264.7 macrophages treated for 4 h with ATP (5 mM), MSU crystals (200 µg/ml), palmitate (1 mM), S100A9 (0.5 µg/ml), IL-6 (0.5 µg/ml), LPS (0.1 µg/ml) or Pam3-CSK_4 (1 µg/ml).

(**D**) Percentage of ASC specking monocytes from p.A439T CAPS patients (grey bars) and healthy donors (blue bars) after whole blood treated during 6 h with $Pam3CSK_4$ (1 µg/ml), IL-6 (0.5 µg/ml), S100A9 (0.5 µg/ml) or palmitate (1 mM).

(**E,F**) ELISA for IL-1β (E) and TNF-α (F) release from healthy donors and p.A439T CAPS patients PBMCs treated as indicated in panel D.

(**G**) Violin plot of *S100A9* mRNA expression from blood cells of healthy individuals or CAPS patients with the p.G569R NLRP3 mutation during active disease or treated with anakinra (using dataset GSE57253). The median indicated by the middle line.

For exact *n* numbers of panels A,B see 'Statistics and reproducibility' section in Methods; for panel C *n*= 3 independent experiments (each one represented by a different symbol); for panels D-F, each dot corresponds to a different donor (*n*=3 healthy donors, *n*=2 CAPS); and for panel G *n*=5 healthy donors, *n*=7 CAPS patients during active disease and the same *n*=7 patients treated with anakinra; For panels A-F data are represented as mean ± SEM; Ordinary one-way ANOVA test for A-C, except for p.T348M mutant in B one-way Kruskal-Wallis; Wald test two-sided with Benjamini–Hochberg correction for G; significance levels are indicated as follows: *p<0.05; *ns* indicates no significant difference (p>0.05). Source data are provided as a Source Data file.

Figure 5. NF-κB induction enhances pathogenic NLRP3 inflammasome activation

(**A**) Western blot for GSDMD, caspase-1 and IL-1β in supernatants from *Nlrp3*$^{-/-}$ immortalized macrophages (iMos) expressing human NLRP3 p.D303N mutant induced after 16 h treatment with doxycycline (1 µg/ml) and palmitate (1 mM), recombinant S100A9 (0.5 µg/ml), recombinant IL-6 (0.5 µg/ml), LPS (0.1 µg/ml) or $Pam3\text{-}CSK_4$ (1 µg/ml).

(**B**) Percentage of ASC specking iMos expressing human NLRP3 p.D303N mutant treated as described in panel A.

(**C-E**) ELISA for the release of IL-18 (C), IL-1α (D), soluble P2X7 receptor (E) from iMos expressing human NLRP3 p.D303N mutant treated as described in panel A, but with or without MCC950 (10 µM).

(**F**) Percentage of extracellular LDH in iMos expressing human NLRP3 p.D303N mutant treated as indicated in panel C.

Western blots are representative of *n*= 3 independent experiments. For panels B-F *n*= 3 independent experiments (each one represented by a different symbol), except for panel C where S100A9 treatment is *n*= 4, and data is presented as mean ± SEM; Ordinary one-way ANOVA test was used for panel B, and *t*-test two-sided in panels C-F; *ns* indicates no significant difference ($p > 0.05$). Source data are provided as a Source Data file.

Figure 6. Deubiquitinases control pathogenic NLRP3 inflammasome activity

(**A**) Western blot for NLRP3, GSDMD and β-actin in cell lysates from *Nlrp3*$^{-/-}$ immortalized macrophages (iMos) expressing the human NLRP3 p.D303N mutant induced after 16 h treatment with doxycycline (1 µg/ml), in the absence or presence of G5 (5 µM), b-AP15 (5 µM) or PR-619 (10 µM).

(**B**) ELISA for IL-18 release from iMos treated as described in panel A.

(**C**) Western blot for NLRP3, GSDMD and β-actin in cell lysates from *Nlrp3*$^{-/-}$ iMos expressing human NLRP3 p.D303N mutant induced after 16 h treatment with doxycycline (1 µg/ml), and then treated for 6 h with LPS (0.1 µg/ml) in the absence or presence of G5 (5 µM), b-AP15 (5 µM) or PR-619 (10 µM).

(**D**) Colorimetric quantification of the levels of secreted alkaline phosphatase (SEAP) from RAW 264.7 macrophages expressing SEAP reporter gen under the control of the NF-κB promoter treated for 6 h with LPS (0.1 µg/ml) in the absence or presence of G5 (5 µM) or b-AP15 (5 µM) or PR619 (10 µM).

(**E-G**) ELISA for TNF-α (E), IL-18 (F) and IL-1β (G) release from iMos treated as described in panel C.

(**H**) Percentage of ASC specking monocytes from CAPS patients after whole blood treated for 6 h with LPS (0.1 µg/ml) in the absence or presence of G5 (5 µM) or b-AP15 (5 µM).

Blots are representative of *n*= 3 independent experiments. For panels D,F *n*= 3 and for panels B,E,G *n*= 4 independent experiments (each one is represented by a different symbol); For panel H each dot corresponds to a different CAPS donor, *n*= 3 patients and each colour represents a different mutation as indicated; Histogram data is represented as mean ± SEM; Ordinary one-way ANOVA test was used for panels D,E,G and *t*-test two-sided was used for panel B,F,H; *ns* indicates no significant difference ($p > 0.05$). Source data are provided as a Source Data file.

Figure 7. Monocytes from CAPS patients present an altered metabolism

(**A**) Principal component analysis (PCA) model plot of metabolomic profiles of monocytes from healthy subjects (*n*= 4) and CAPS (*n*= 4) incubated or not for 2h with LPS (500 ng/ml).

(**B**) Metabolomic profiles of monocytes from healthy subjects (average of *n*= 4) and CAPS (average of *n*= 4) incubated or not for 2h with LPS (500 ng/ml).

(**C**) Volcano plots of blood monocytes from healthy subjects (*n*= 4) and CAPS patients (*n*= 4), with expression (log_2 values) plotted against the adjusted P value for the difference metabolite abundance, *t*-test two-sided. Significantly upregulated (red) or downregulated (blue) metabolites one-fold or more in monocytes from CAPS patients relative to that in monocytes from healthy subjects.

(**D**) Violin plot of mRNA expression from genes of the glycolysis (*BPGM, ENO3, LDHA, PFKFB3*) and pentose phosphate pathway (*DERA*, *PGM2*, *NAMPT*) from blood cells of healthy donors (HD) or CAPS patients with p.G569R NLRP3 mutation during active disease or after treatment with anakinra (Ank) (using dataset GSE57253). Middle dotted line depicts the median and graphic represents data from *n*= 5 healthy donors, *n*= 7 CAPS patients during active disease and the same *n*= 7 CAPS patients CAPS treated

with anakinra; Wald test two-sided, with Benjamini–Hochberg correction, were used to compare gene expression.

(**E**) Boxplot of mRNA expression from genes of the glycolysis (*Bpgm, Eno3, Ldha, Pfkfb3*) and pentose phosphate pathway (*Dera*, *Pgm2*, *Nampt*) from *Nlrp3*$^{-/-}$ immortalized macrophages treated for 16 h with or without doxycycline (1 µg/ml) to induce the expression of human NLRP3 p.D303N variant in absence/presence of MCC950 (10 µM). Middle line depicts the mean, error bars represent minimum and maximum, and bounds of box represent the 25th to 75th percentile respectively; graphic represents data from *n*= 4 independent experiments. Source data are provided as a Source Data file.

Figure 8. Transcriptomic analysis of macrophages expressing the pathogenic NLRP3 p.D303N variant

(**A**) Gene expression profile of *Nlrp3*$^{-/-}$ immortalized macrophages (iMos) treated for 16 h with or without doxycycline (1 µg/ml) to induce the expression of the human NLRP3 p.D303N variant, in the absence or presence of MCC950 (10 µM). The grey boxes on the right highlight some of the genes or pathways identified in each trend. The data represented in the graphics are derived from four independent experiments.

(**B**) Relative expression of glycolysis genes from iMos treated as described in panel A, but expressing either wild-type NLRP3 or the p.D303N variant. The data are represented as circles, where the size indicates the fold change of doxycycline treated cells vs untreated cells, and doxycycline with MCC950 treatment vs doxycycline, and the color represents the *t*-test two-sided $-\text{Log}_{10}$ *p*-value (the dotted line in the color scale represents *p*= 0.05). The graphics represent data from three to four independent experiments.

(**C**) Gene ontology for biological process enrichment analysis of differentially expressed genes from *Nlrp3*$^{-/-}$ iMos treated as described in panel A. The data are represented as circles, where the size indicates the gene count for that particular process, and the color

represents the $-\text{Log}_{10}$ *p*-value calculated with one-sided Fisher's Exact test with Benjamini–Hochberg correction (the dotted line in the color scale represents *p*= 0.05). The graphics represent data from four independent experiments. Source data are provided as a Source Data file.

Figure 9. Decreased glycolytic capacity of macrophages expressing the pathogenic NLRP3 p.D303N variant

(**A,B**) Seahorse analysis of glycolysis in *Nlrp3*$^{-/-}$ immortalized macrophages (iMos) treated for 16 h with or without doxycycline (1 µg/ml) to induce the expression of the human NLRP3 p.D303N variant, in the absence or presence of MCC950 (10 µM) and LPS (100 ng/ml). In panel B iMos were not expressing NLRP3 (white) or expressed either the human NLRP3 wild type (blue) or the p.D303N variant (grey).

(**C**) Measurement of L-Lactate in the supernatants from iMos treated as described in panel A.

(**D**) Seahorse analysis of glycolytic ATP and mitochondrial ATP production rates from iMos treated as described in panel A. The darker columns represent glycolytic ATP, and the lighter columns represent mitochondrial ATP.

(**E**) Seahorse analysis of mitochondria activity measuring basal and maximal respiration from iMos treated as described in panel A.

Data are represented as mean ± SEM; For panel A data are derived from *n*= 7 biological replicates, which are representative of *n*= 4 independent experiments. For panel B,D,E *n*= 3 biological replicates for empty vector and wild type NLRP3 (representative of *n*= 3 independent experiments) and *n*= 7 biological replicates for NLRP3 p.D303N, except *n*= 6 in untreated conditions for maximal respiration in panel E (representative of *n*= 4 independent experiments). For panel C *n*= 3 independent experiments. *t*-test two-sided was used in panels C-E and ordinary one-way ANOVA test was used for panel B; *ns*

indicates no significant difference (p> 0.05). In panel D, blue represent statistics from mitochondrial ATP and grey represents statistics from glycolytic ATP. Source data are provided as a Source Data file.

Figure 10. Glycolysis modulates the release of IL-1β, but not IL-18, in macrophages expressing NLRP3 p.D303N

(**A**) ELISA for IL-1β and IL-18 from *Nlrp3*$^{-/-}$ immortalized macrophages (iMos) treated for 16 h with or without doxycycline (1 µg/ml) to induce the expression of either the human wild type NLRP3 or the p.D303N variant, in the absence or presence of MCC950 (10 µM) and pyruvate (10 mM). The data are derived from *n*= 3 independent experiments.

(**B**) Box plot of *Il1b* mRNA expression from *Nlrp3*$^{-/-}$ iMos treated as described in panel A, but were expressing either wild type NLRP3 or the p.D303N variant and were treated with or without LPS (100 ng/ml). Middle line depicts the mean, error bars represent minimum and maximum, and bounds of box represent the 25th to 75th percentile respectively; graphic represents data from *n*= 4 independent experiments, except for NLRP3 wild type untreated and doxycycline+MCC950 treatment that were *n*= 3 independent experiments.

(**C**) ELISA for IL-1β and IL-18 from *Nlrp3*$^{-/-}$ iMos expressing either the human wild type NLRP3 or the p.D303N variant induced after treatment for 4 h with doxycycline (1 µg/ml) in the absence or presence of LPS (100 ng/ml), MCC950 (10 µM) and 2-DG (0.1, 0.5 and 1 mM). The data are derived from *n*= 3 independent experiments.

Data are represented as mean ± SEM; a *t*-test two-sided was used in panels A-C; *ns* indicates no significant difference (p> 0.05). Source data are provided as a Source Data file.

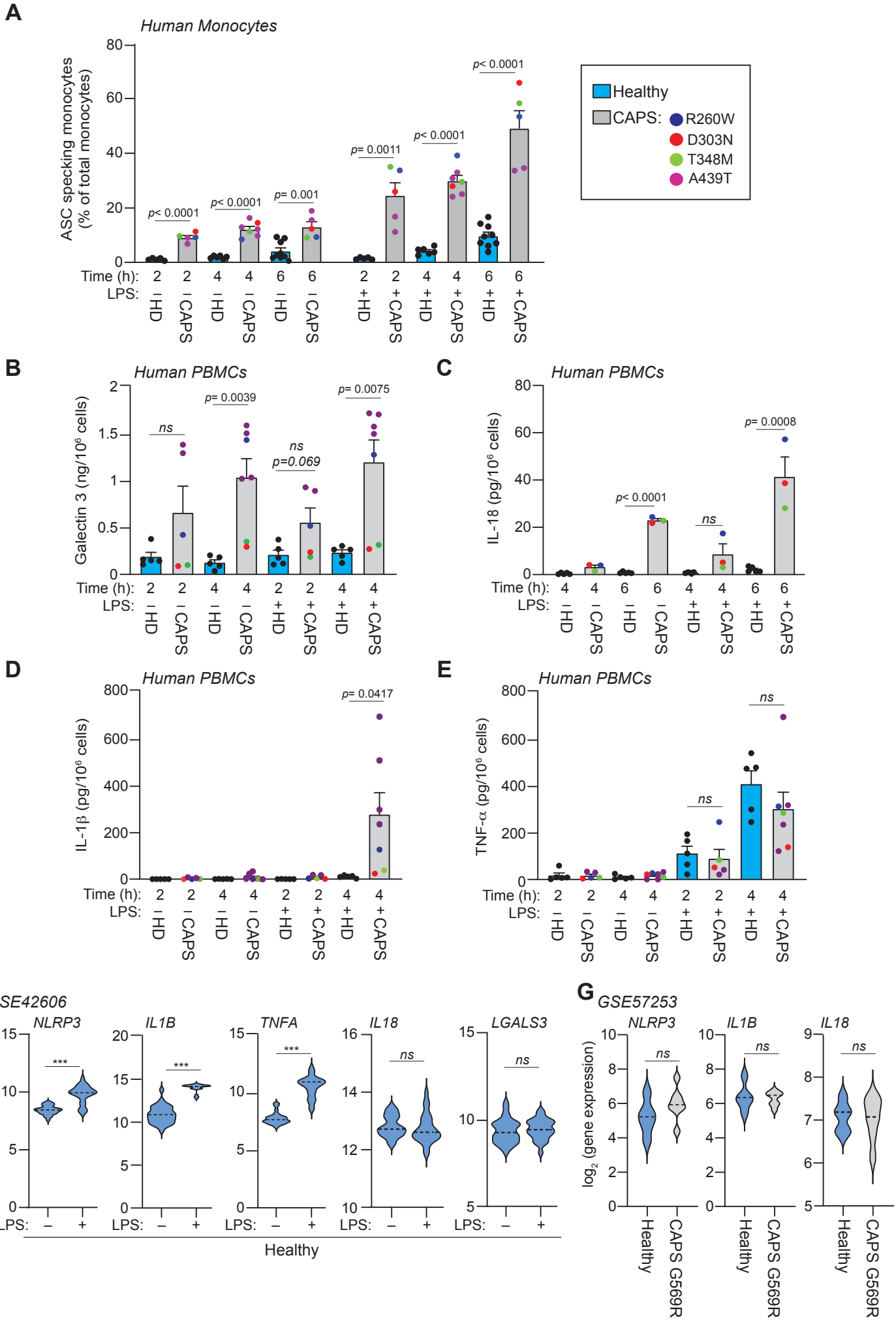
A
Human Monocytes
ASC specking monocytes (% of total monocytes)
Healthy
CAPS:
R260W
D303N
T348M
A439T
p< 0.0001
p< 0.0001
p= 0.001
p= 0.0011
p< 0.0001
p< 0.0001
Time (h):
LPS:
HD
CAPS
B
Human PBMCs
Galectin 3 (ng/10^6 cells)
ns
p= 0.0039
ns
p=0.069
p= 0.0075
C
Human PBMCs
IL-18 (pg/10^6 cells)
p< 0.0001
ns
p= 0.0008
D
Human PBMCs
IL-1β (pg/10^6 cells)
p= 0.0417
E
Human PBMCs
TNF-α (pg/10^6 cells)
ns
ns
ns
F
GSE42606
NLRP3
IL1B
TNFA
IL18
LGALS3
log2 (gene expression)
***
***
ns
ns
ns
LPS:
Healthy
G
GSE57253
NLRP3
IL1B
IL18
log2 (gene expression)
ns
ns
ns
Healthy
CAPS G569R

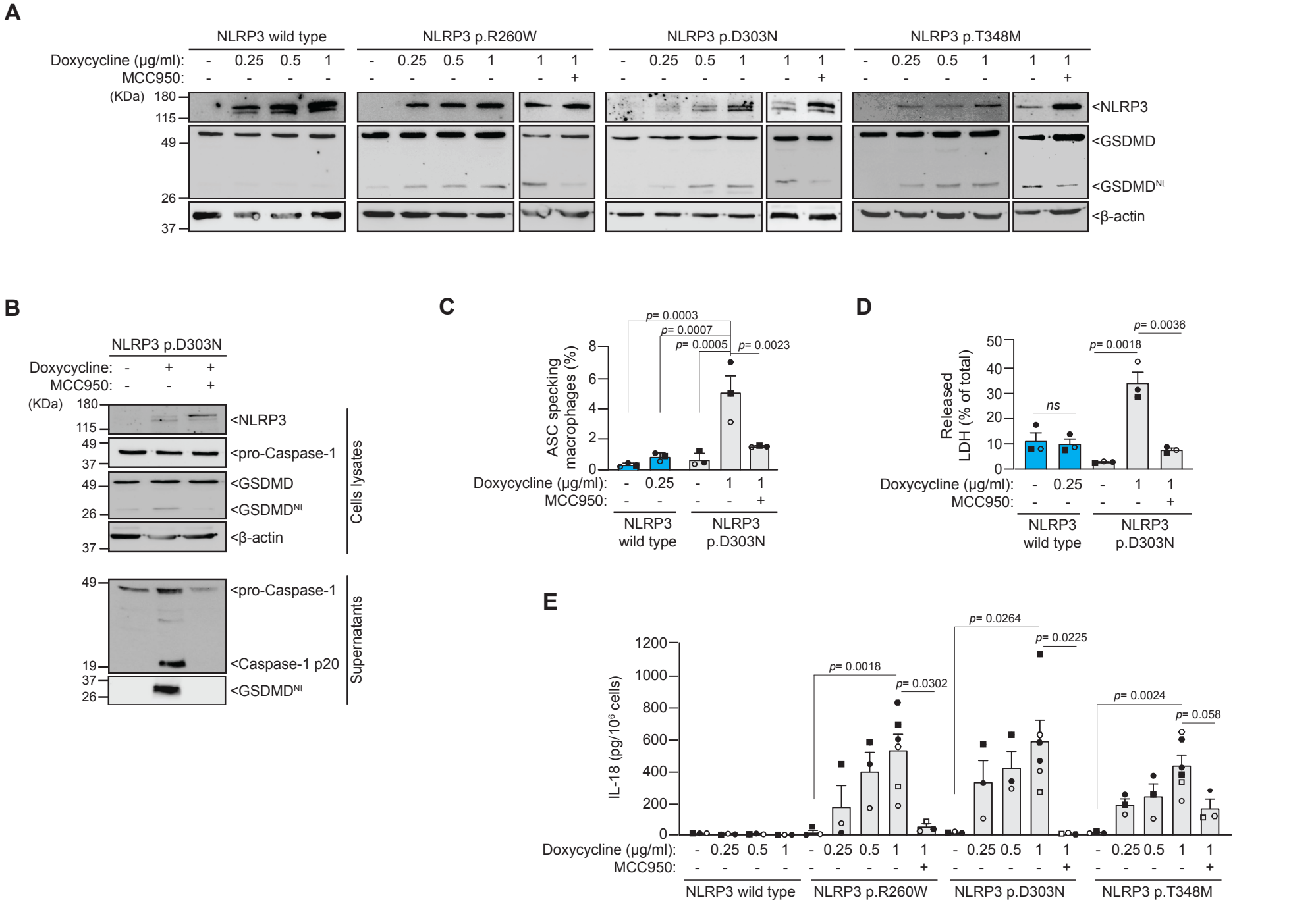
A
NLRP3 wild type
NLRP3 p.R260W
NLRP3 p.D303N
NLRP3 p.T348M
Doxycycline (µg/ml):
MCC950:
(KDa)
180
115
49
26
37
<NLRP3
<GSDMD
<GSDMD^Nt
<β-actin
B
NLRP3 p.D303N
Doxycycline:
MCC950:
<pro-Caspase-1
<Caspase-1 p20
Cells lysates
Supernatants
C
ASC specking macrophages (%)
p= 0.0003
p= 0.0007
p= 0.0005
p= 0.0023
NLRP3 wild type
NLRP3 p.D303N
D
Released LDH (% of total)
ns
p= 0.0018
p= 0.0036
E
IL-18 (pg/10^6 cells)
p= 0.0018
p= 0.0302
p= 0.0264
p= 0.0225
p= 0.0024
p= 0.058
NLRP3 wild type
NLRP3 p.R260W
NLRP3 p.D303N
NLRP3 p.T348M

Figure 3

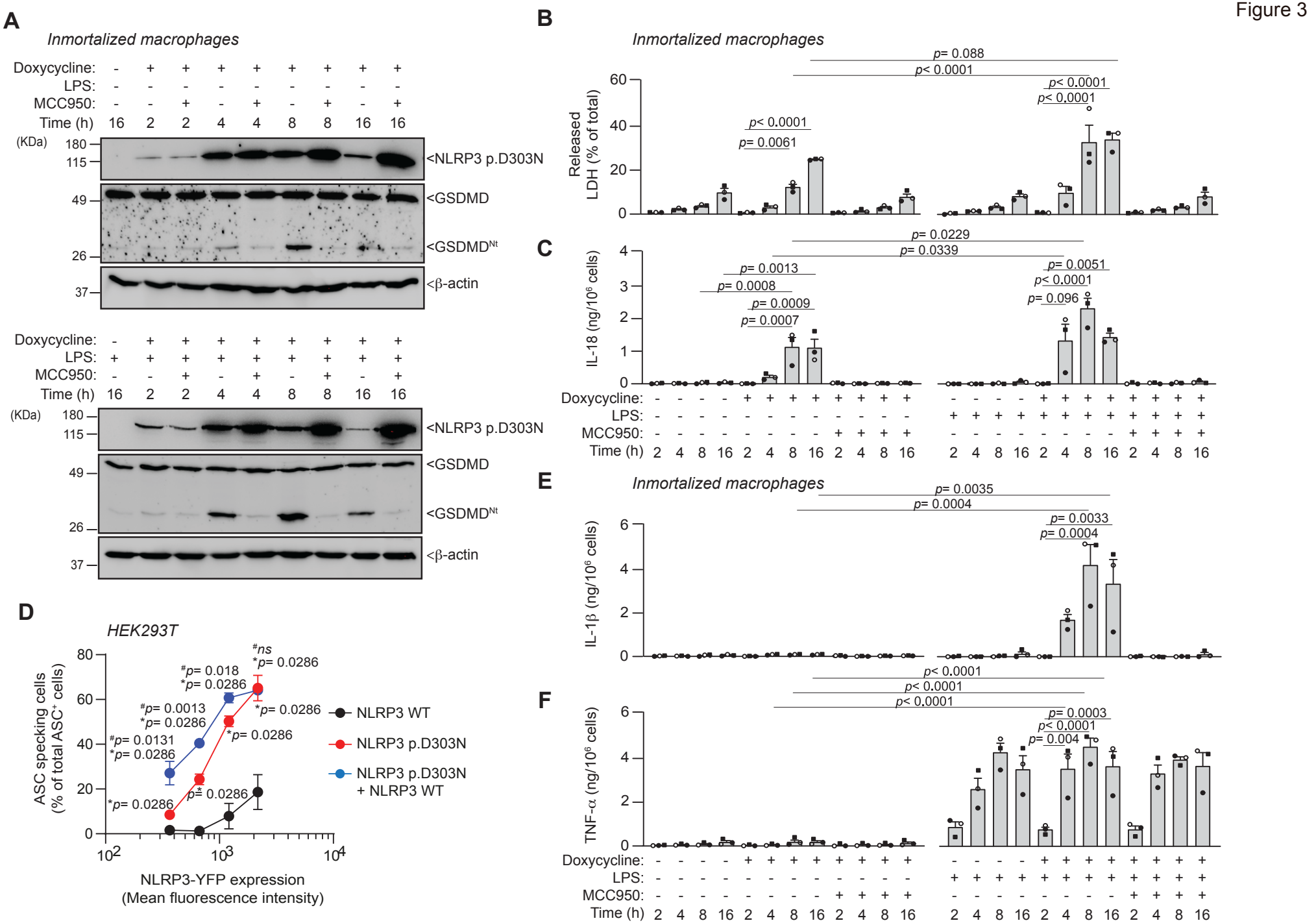
A
Inmortalized macrophages
Doxycycline:
LPS:
MCC950:
Time (h)
(KDa)
<NLRP3 p.D303N
<GSDMD
<GSDMD^Nt
<β-actin
B
Inmortalized macrophages
Released LDH (% of total)
C
IL-18 (ng/10^6 cells)
E
Inmortalized macrophages
IL-1β (ng/10^6 cells)
F
TNF-α (ng/10^6 cells)
D
HEK293T
ASC specking cells (% of total ASC+ cells)
NLRP3-YFP expression (Mean fluorescence intensity)
NLRP3 WT
NLRP3 p.D303N
NLRP3 p.D303N + NLRP3 WT

Figure 4

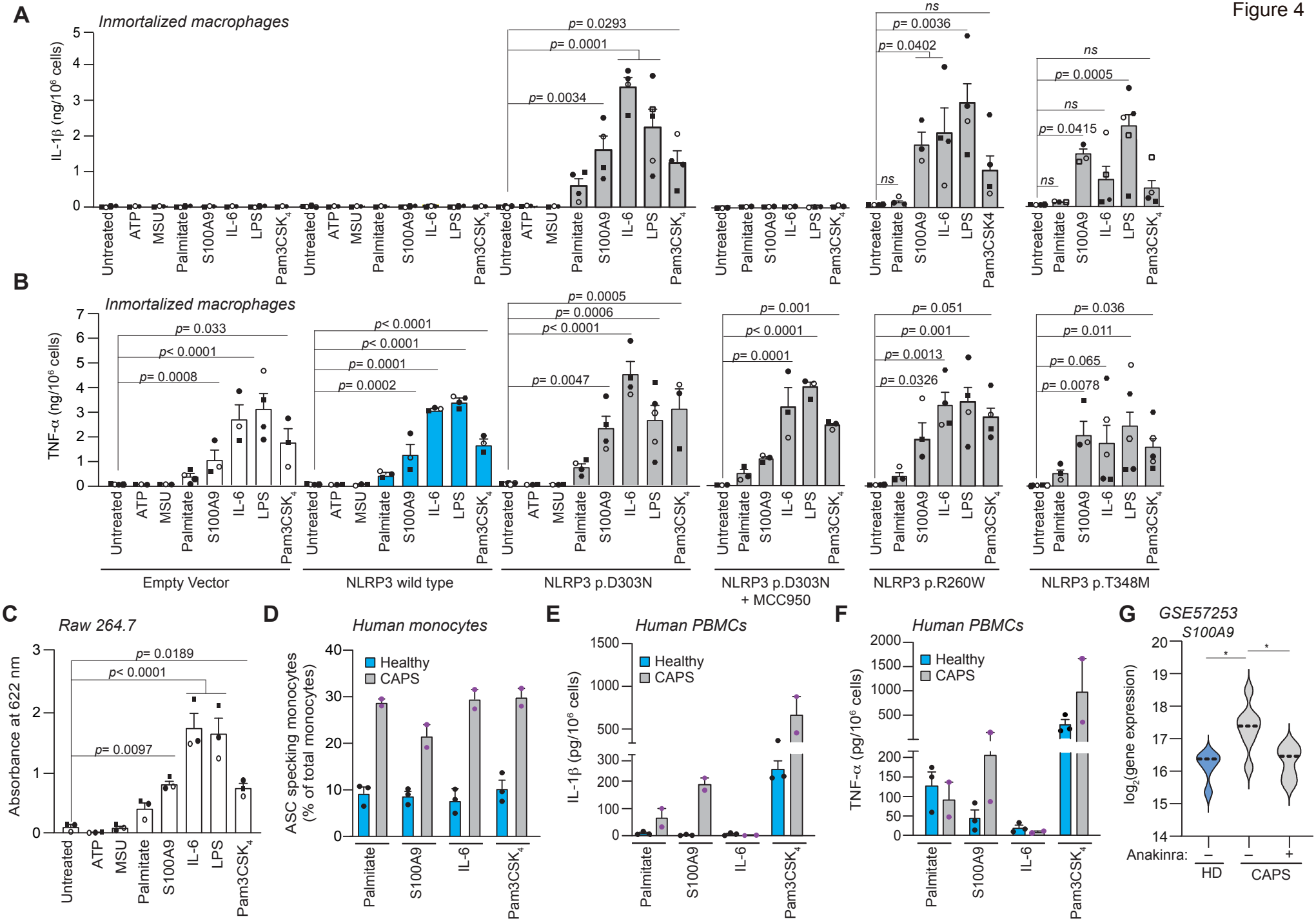
A
Inmortalized macrophages
IL-1β (ng/10⁶ cells)
p= 0.0293
p= 0.0001
p= 0.0034
ns
p= 0.0036
p= 0.0402
ns
p= 0.0005
ns
p= 0.0415
ns
Untreated
ATP
MSU
Palmitate
S100A9
IL-6
LPS
Pam3CSK4
B
Inmortalized macrophages
TNF-α (ng/10⁶ cells)
p= 0.033
p< 0.0001
p= 0.0008
p< 0.0001
p< 0.0001
p= 0.0001
p= 0.0002
p= 0.0005
p= 0.0006
p< 0.0001
p= 0.0047
p= 0.001
p< 0.0001
p= 0.0001
p= 0.051
p= 0.001
p= 0.0013
p= 0.0326
p= 0.036
p= 0.011
p= 0.065
p= 0.0078
Empty Vector
NLRP3 wild type
NLRP3 p.D303N
NLRP3 p.D303N + MCC950
NLRP3 p.R260W
NLRP3 p.T348M
C
Raw 264.7
Absorbance at 622 nm
p= 0.0189
p< 0.0001
p= 0.0097
D
Human monocytes
ASC specking monocytes (% of total monocytes)
Healthy
CAPS
E
Human PBMCs
IL-1β (pg/10⁶ cells)
F
Human PBMCs
TNF-α (pg/10⁶ cells)
G
GSE57253
S100A9
log2(gene expression)
Anakinra:
HD
CAPS

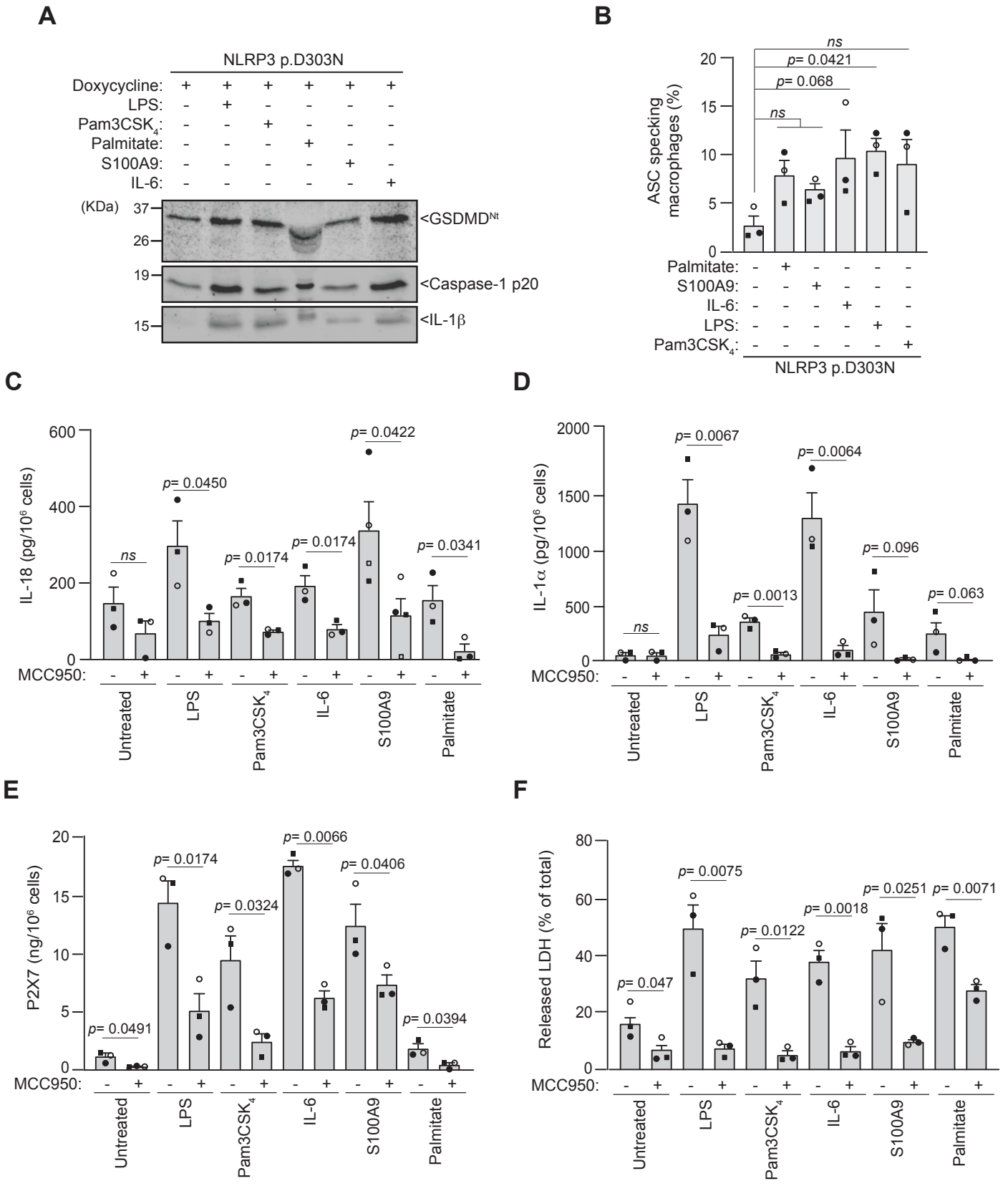
A
NLRP3 p.D303N
Doxycycline:
LPS:
Pam3CSK4:
Palmitate:
S100A9:
IL-6:
(KDa)
37
26
19
15
<GSDMDNt
<Caspase-1 p20
<IL-1β
B
ASC specking macrophages (%)
ns
p= 0.0421
p= 0.068
ns
Palmitate:
S100A9:
IL-6:
LPS:
Pam3CSK4:
NLRP3 p.D303N
C
IL-18 (pg/10^6 cells)
ns
p= 0.0450
p= 0.0174
p= 0.0174
p= 0.0422
p= 0.0341
MCC950:
Untreated
LPS
Pam3CSK4
IL-6
S100A9
Palmitate
D
IL-1α (pg/10^6 cells)
ns
p= 0.0067
p= 0.0013
p= 0.0064
p= 0.096
p= 0.063
E
P2X7 (ng/10^6 cells)
p= 0.0491
p= 0.0174
p= 0.0324
p= 0.0066
p= 0.0406
p= 0.0394
F
Released LDH (% of total)
p= 0.047
p= 0.0075
p= 0.0122
p= 0.0018
p= 0.0251
p= 0.0071

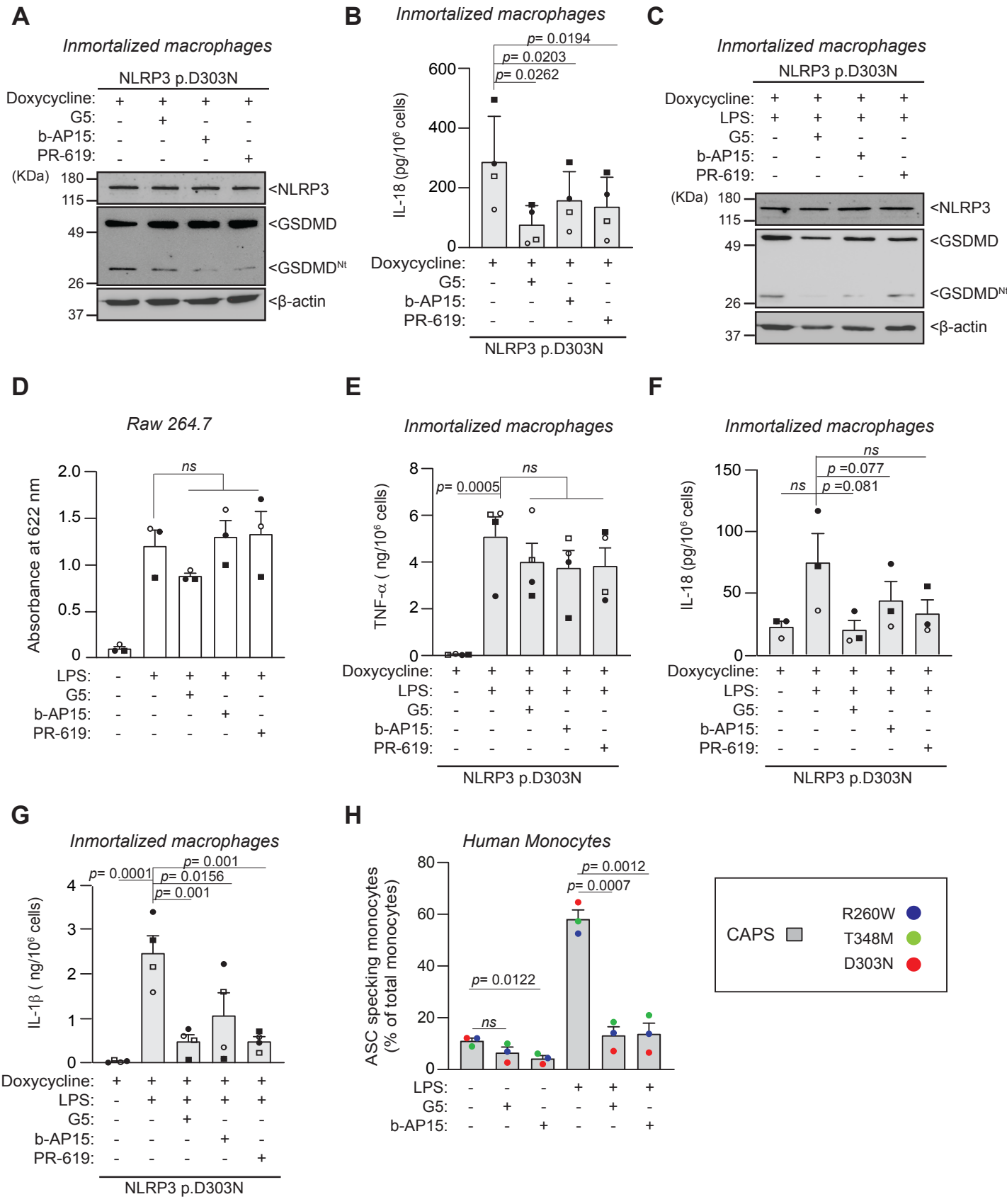
A
Inmortalized macrophages
NLRP3 p.D303N
Doxycycline: + + + +
G5: - + - -
b-AP15: - - + -
PR-619: - - - +
(KDa) 180
115
49
26
37
<NLRP3
<GSDMD
<GSDMDNt
<β-actin
B
Inmortalized macrophages
p= 0.0194
p= 0.0203
p= 0.0262
IL-18 (pg/10^6 cells)
600
400
200
0
Doxycycline: + + + +
G5: - + - -
b-AP15: - - + -
PR-619: - - - +
NLRP3 p.D303N
C
Inmortalized macrophages
NLRP3 p.D303N
Doxycycline: + + + +
LPS: + + + +
G5: - + - -
b-AP15: - - + -
PR-619: - - - +
(KDa) 180
115
49
26
37
<NLRP3
<GSDMD
<GSDMDNt
<β-actin
D
Raw 264.7
Absorbance at 622 nm
2.0
1.5
1.0
0.5
0
ns
LPS: - + + + +
G5: - - + - -
b-AP15: - - - + -
PR-619: - - - - +
E
Inmortalized macrophages
TNF-α (ng/10^6 cells)
8
6
4
2
0
p= 0.0005
ns
Doxycycline: + + + + +
LPS: - + + + +
G5: - - + - -
b-AP15: - - - + -
PR-619: - - - - +
NLRP3 p.D303N
F
Inmortalized macrophages
IL-18 (pg/10^6 cells)
150
100
50
0
ns
p =0.077
ns
p =0.081
Doxycycline: + + + + +
LPS: - + + + +
G5: - - + - -
b-AP15: - - - + -
PR-619: - - - - +
NLRP3 p.D303N
G
Inmortalized macrophages
IL-1β (ng/10^6 cells)
4
3
2
1
0
p= 0.0001
p= 0.001
p= 0.0156
p= 0.001
Doxycycline: + + + + +
LPS: - + + + +
G5: - - + - -
b-AP15: - - - + -
PR-619: - - - - +
NLRP3 p.D303N
H
Human Monocytes
ASC specking monocytes (% of total monocytes)
80
60
40
20
0
p= 0.0012
p= 0.0007
p= 0.0122
ns
LPS: - - - + + +
G5: - + - - + -
b-AP15: - - + - - +
CAPS
R260W
T348M
D303N

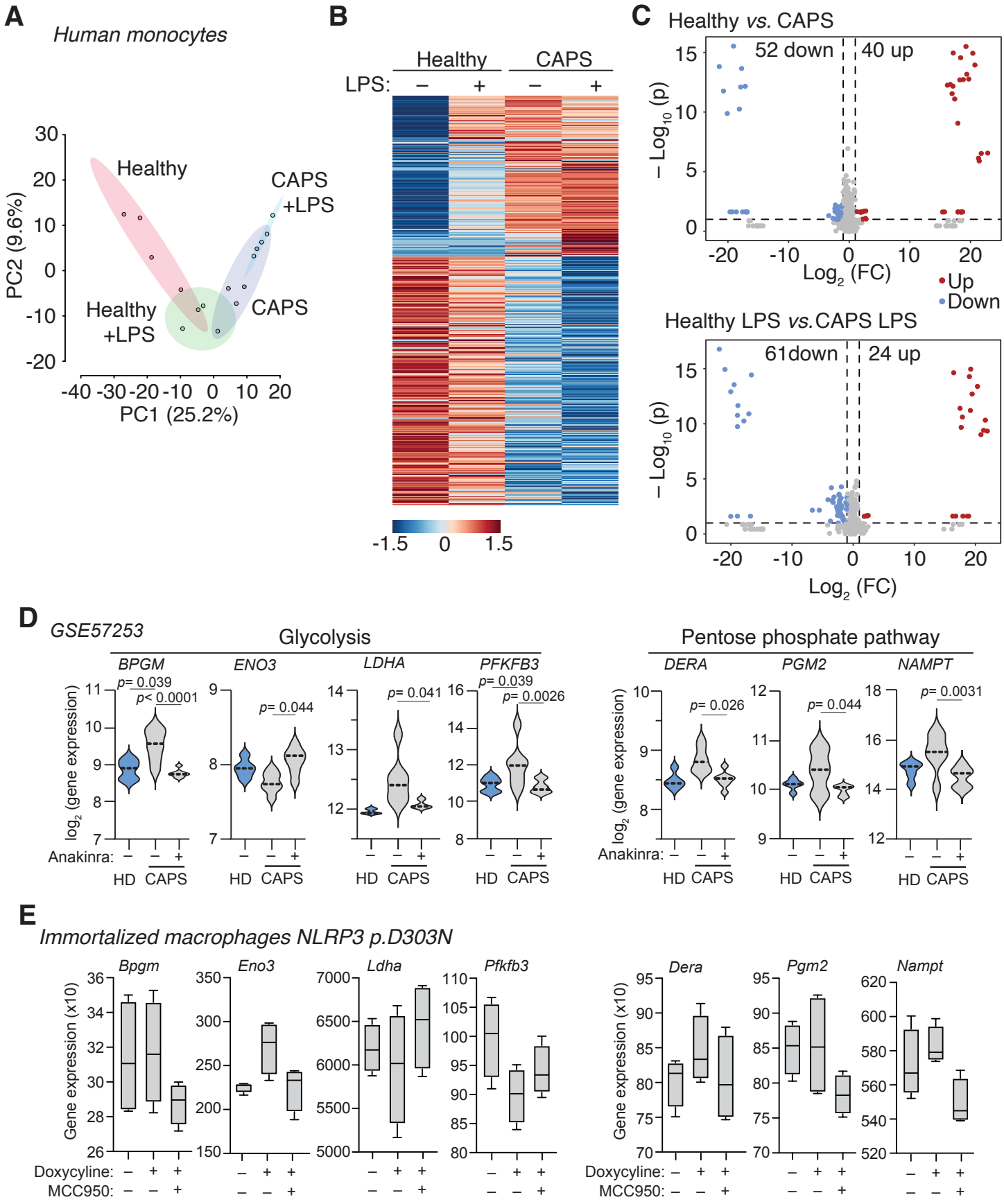
A
Human monocytes
Healthy
CAPS +LPS
Healthy +LPS
CAPS
PC2 (9.6%)
PC1 (25.2%)
B
Healthy
CAPS
LPS: – + – +
-1.5 0 1.5
C
Healthy vs. CAPS
52 down
40 up
– Log10 (p)
Log2 (FC)
Up
Down
Healthy LPS vs. CAPS LPS
61down
24 up
D
GSE57253
Glycolysis
Pentose phosphate pathway
BPGM
ENO3
LDHA
PFKFB3
DERA
PGM2
NAMPT
p= 0.039
p< 0.0001
p= 0.044
p= 0.041
p= 0.039
p= 0.0026
p= 0.026
p= 0.044
p= 0.0031
log2 (gene expression)
Anakinra: – – +
HD CAPS
E
Immortalized macrophages NLRP3 p.D303N
Bpgm
Eno3
Ldha
Pfkfb3
Dera
Pgm2
Nampt
Gene expression (x10)
Doxycyline: – + +
MCC950: – – +

Figure 8

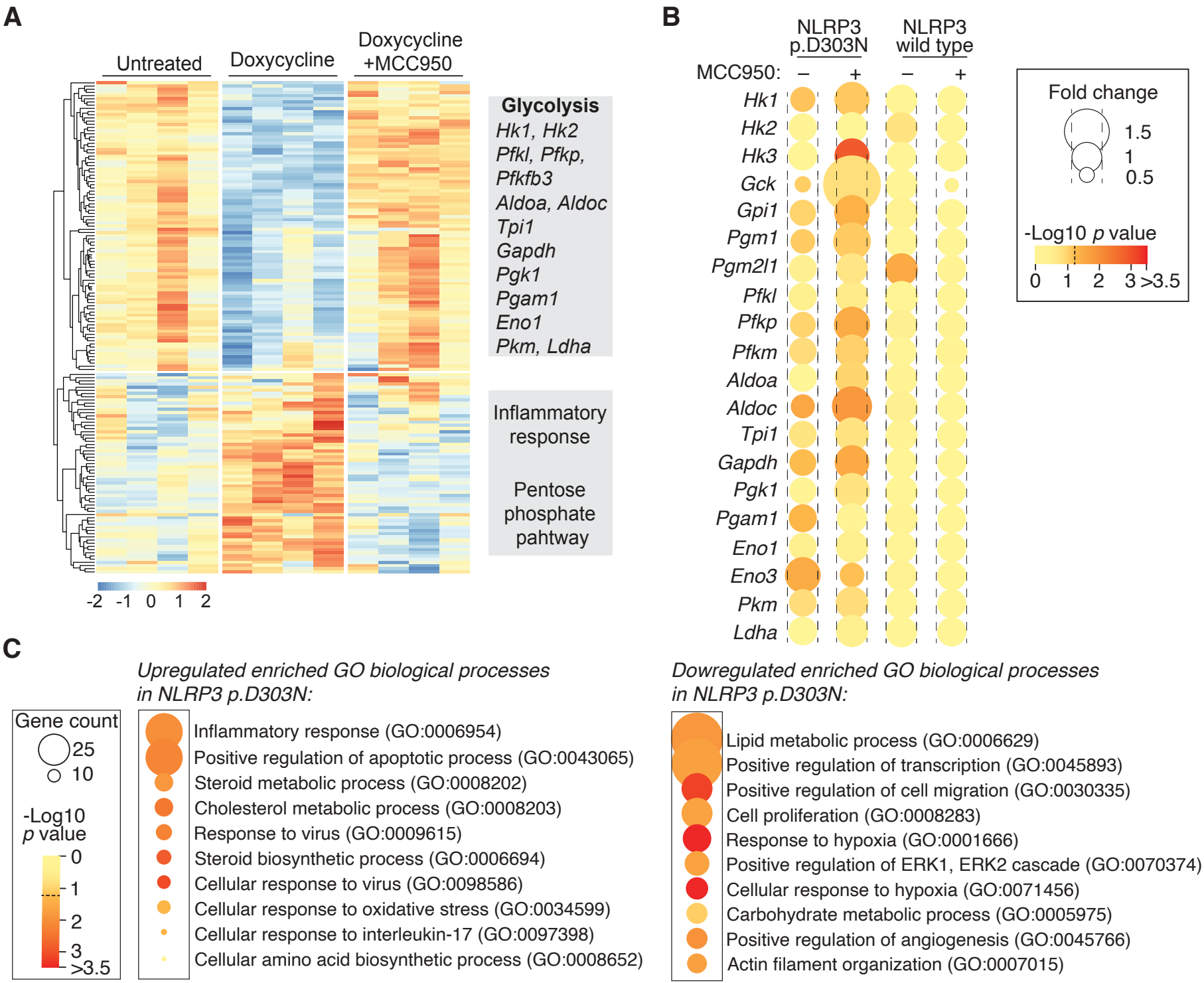
A
Untreated
Doxycycline
Doxycycline +MCC950
-2 -1 0 1 2
Glycolysis
Hk1, Hk2
Pfkl, Pfkp,
Pfkfb3
Aldoa, Aldoc
Tpi1
Gapdh
Pgk1
Pgam1
Eno1
Pkm, Ldha
Inflammatory response
Pentose phosphate pahtway
B
NLRP3 p.D303N
NLRP3 wild type
MCC950: – + – +
Hk1
Hk2
Hk3
Gck
Gpi1
Pgm1
Pgm2l1
Pfkl
Pfkp
Pfkm
Aldoa
Aldoc
Tpi1
Gapdh
Pgk1
Pgam1
Eno1
Eno3
Pkm
Ldha
Fold change
1.5
1
0.5
-Log10 p value
0 1 2 3 >3.5
C
Upregulated enriched GO biological processes in NLRP3 p.D303N:
Gene count
25
10
-Log10 p value
0
1
2
3
>3.5
Inflammatory response (GO:0006954)
Positive regulation of apoptotic process (GO:0043065)
Steroid metabolic process (GO:0008202)
Cholesterol metabolic process (GO:0008203)
Response to virus (GO:0009615)
Steroid biosynthetic process (GO:0006694)
Cellular response to virus (GO:0098586)
Cellular response to oxidative stress (GO:0034599)
Cellular response to interleukin-17 (GO:0097398)
Cellular amino acid biosynthetic process (GO:0008652)
Dowregulated enriched GO biological processes in NLRP3 p.D303N:
Lipid metabolic process (GO:0006629)
Positive regulation of transcription (GO:0045893)
Positive regulation of cell migration (GO:0030335)
Cell proliferation (GO:0008283)
Response to hypoxia (GO:0001666)
Positive regulation of ERK1, ERK2 cascade (GO:0070374)
Cellular response to hypoxia (GO:0071456)
Carbohydrate metabolic process (GO:0005975)
Positive regulation of angiogenesis (GO:0045766)
Actin filament organization (GO:0007015)

Figure 9

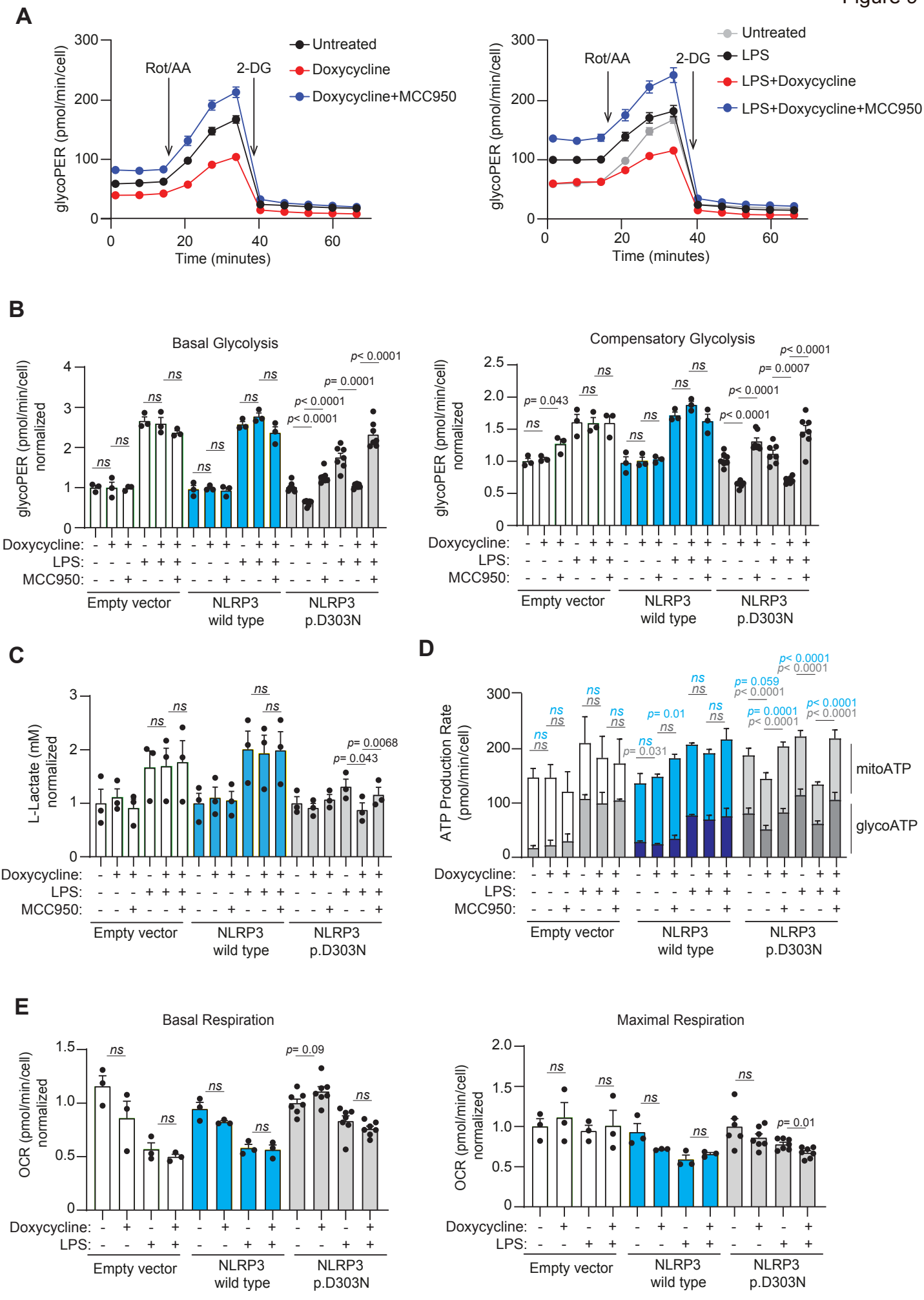
A
glycoPER (pmol/min/cell)
Time (minutes)
Rot/AA
2-DG
Untreated
Doxycycline
Doxycycline+MCC950
LPS
LPS+Doxycycline
LPS+Doxycycline+MCC950
B
Basal Glycolysis
Compensatory Glycolysis
glycoPER (pmol/min/cell) normalized
Doxycycline:
LPS:
MCC950:
Empty vector
NLRP3 wild type
NLRP3 p.D303N
C
L-Lactate (mM) normalized
D
ATP Production Rate (pmol/min/cell)
mitoATP
glycoATP
E
Basal Respiration
Maximal Respiration
OCR (pmol/min/cell) normalized

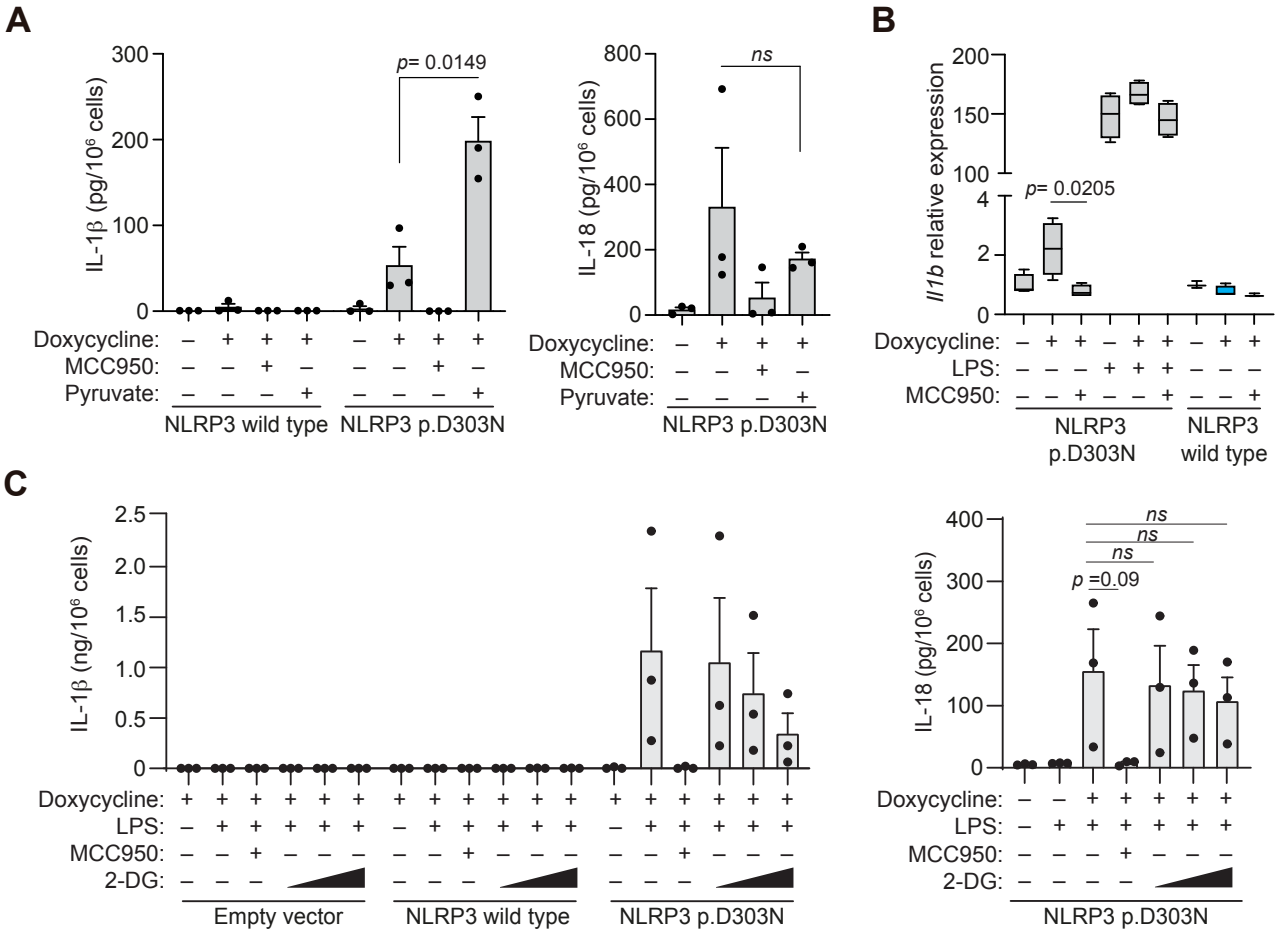
A
IL-1β (pg/10⁶ cells)
p= 0.0149
Doxycycline:
MCC950:
Pyruvate:
NLRP3 wild type
NLRP3 p.D303N
IL-18 (pg/10⁶ cells)
ns
B
Il1b relative expression
p= 0.0205
LPS:
NLRP3 p.D303N
NLRP3 wild type
C
IL-1β (ng/10⁶ cells)
2-DG:
Empty vector
IL-18 (pg/10⁶ cells)
p =0.09

Pathogenic NLRP3 mutants forms constitutively active inflammasomes resulting in immune-metabolic limitation of IL-1β production

Cristina Molina-López, Laura Hurtado-Navarro, Carlos J. García, Diego Angosto-Bazarra, Fernando Vallejo, Ana Tapia-Abellán, Joana R. Marques-Soares, Carmen Vargas, Segundo Bujan-Rivas, Francisco A. Tomás-Barberán, Juan I. Arostegui, Pablo Pelegrin

SUPPLEMENTARY FIGURES

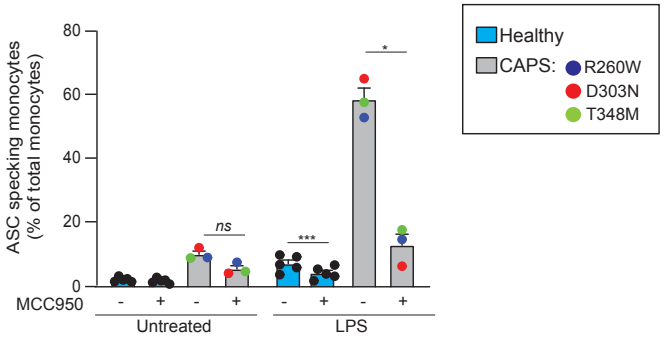

Supplementary Figure 1. Monocytes from CAPS patients show a constitutive activation of the NLRP3 inflammasome
Percentage of ASC specking monocytes from healthy donors (blue bars, *n*= 5) and CAPS patients (grey bars, p.R260W, p.D303N and p.T348M, *n*= 1 each variant, represented by a different color) after whole blood treated or not for 6 h with LPS (0.1 μg/ml), in the presence or absence of MCC950 (10 μM). *t*-test two-sided was performed to compare between MCC950 treated and untreated groups; significance levels are indicated as follows: *p < 0.05; ***p < 0.0002; *ns* indicates no significant difference (p > 0.05). Source data are provided as a Source Data file.

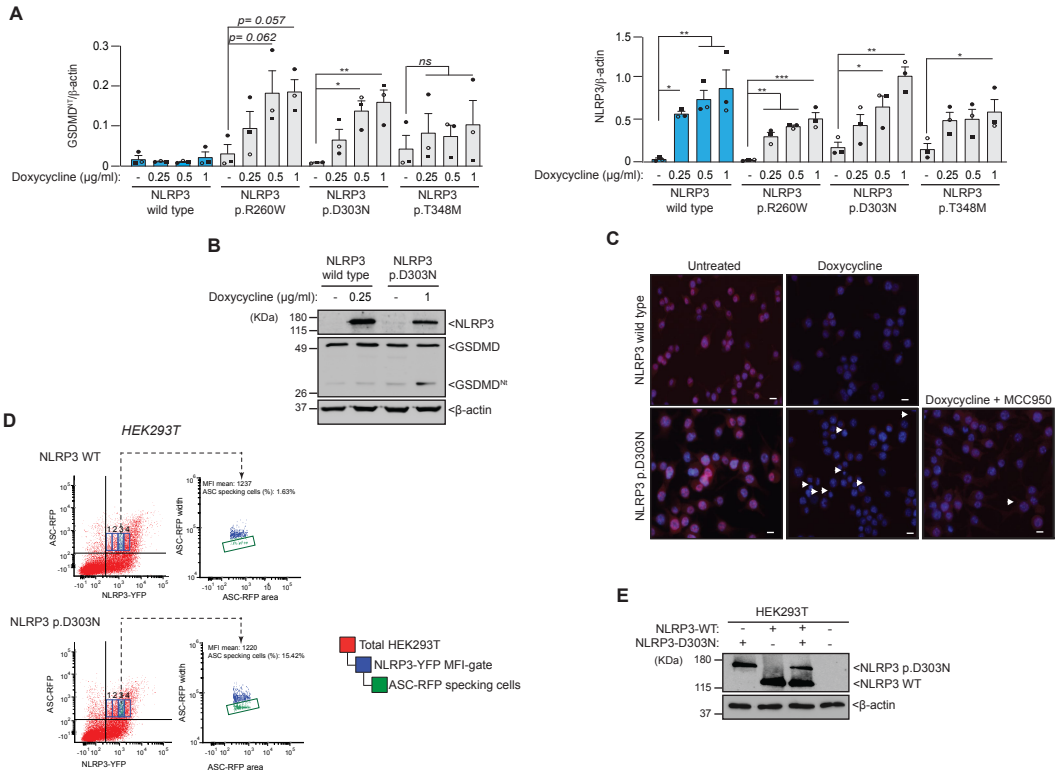

Supplementary Figure 2. Expression of CAPS-associated NLRP3 variants in macrophages results in a constitutive active inflammasome.

(**A**) Ratio of $GSDMD^{NT}$/β-actin (left) or NLRP3/β-actin (right) from Western blots as the ones presented in Figure 1A; *n*= 3 different Western blots corresponding to independent experiments.

(**B**) Western blot for NLRP3, GSDMD, and β-actin in cell lysates from *Nlrp3*$^{-/-}$ immortalized macrophages (iMos) treated for 16 h with or without doxycycline (0.25 or 1 μg/ml) to respectively induce the expression of the human wild type NLRP3 or the p.D303N variant.

(**C**) Representative fluorescence images of *Nlrp3*$^{-/-}$ iMos as the ones quantified in Figure 1C; ASC is shown in red, DAPI is shown in blue; scale bar=10 μm; arrowheads denote ASC specks. Images are representative of *n*= 3 independent experiments.

(**D**) Gating strategy to analyse the percentage of ASC specking cells in four different gates with increased expression of NLRP3-YFP wild type (WT, top) or p.D303N (bottom) calculated as mean fluorescence intensity (MFI). As example, the percentage of ASC specking cells is shown in the gate number three for NLRP3 expression.

(**E**) Western blot for NLRP3 and β-actin in cell lysates from HEK293T transfected with empty vector, NLRP3 wild type (WT), NLRP3 p.D303N-YFP or co-transfected with NLRP3 WT and NLRP3 p.D303N-YFP.

Western blots are representative of *n*= 3 independent experiments each. Graphics are representative of *n*= 3 independent experiments (each one represented by a different symbol) and data is represented as mean ± SEM; Ordinary one-way ANOVA test was used in panel A; significance levels are indicated as follows: * $p < 0.05$; **$p < 0.0021$; *ns* indicates no significant difference ($p > 0.05$). Source data are provided as a Source Data file.

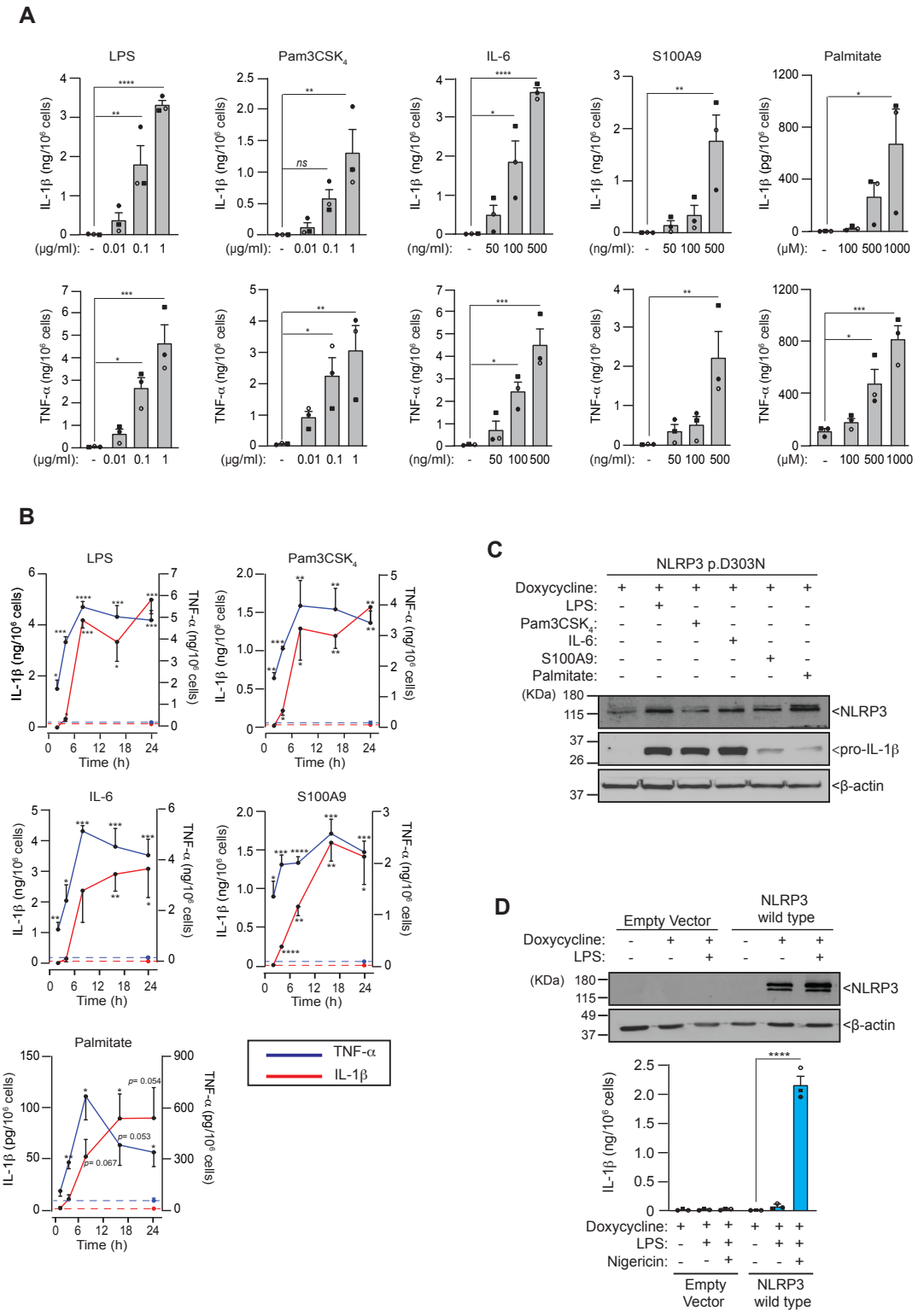

Supplementary Figure 3. NF-κB induction induces IL-1β release from macrophages expressing CAPS-associated NLRP3 variants.
(**A**) ELISA for IL-1β (top) and TNF-α (bottom) release from *Nlrp3*$^{-/-}$ immortalized macrophages (iMos) expressing the human NLRP3 p.D303N mutant induced after 16 h treatment with doxycycline (1 μg/ml) and different concentrations (as annotated) of LPS, Pam3-CSK$_4$, recombinant IL-6, recombinant S100A9 or palmitate.

(**B**) ELISA for IL-1β (red line) and TNF-α (blue line) release from *Nlrp3*$^{-/-}$ iMos treated as indicated in A but for different times (0, 2, 4, 8, 16 and 24 h). The concentrations used were LPS 0.1 µg/ml, Pam3CSK$_4$ 1 µg/ml, recombinant IL-6 0.5 µg/ml, recombinant S100A9 0.5 µg/ml, and palmitate 1 mM. Dotted lines indicate basal cytokine release of IL-1β (red line) or TNF-α (blue line) in untreated iMos cultured for 24h.
(**C**) Western blot for NLRP3, IL-1β and β-actin in cell lysates from *Nlrp3*$^{-/-}$ iMos expressing the human NLRP3 p.D303N mutant induced after 16 h treatment with doxycycline (1 µg/ml) and palmitate (1 mM), recombinant S100A9 (0.5 µg/ml), recombinant IL-6 (0.5 µg/ml), LPS (0.1 µg/ml) or Pam3-CSK$_4$ (1 µg/ml).
(**D**) ELISA for IL-1β release or Western blot for NLRP3 and β-actin in cell lysates from *Nlrp3*$^{-/-}$ iMos transduced with an empty vector or a vector expressing the wild type NLRP3 after 16 h with or without doxycycline (1 µg/ml) and LPS (100 ng/ml), and then for the ELISA treated for additional 30 min with nigericin (10 µM) as indicated. Western blots are representative of *n*= 3 independent experiments; Graphics average *n*= 3 independent experiments (each one represented by a different symbol) and data is represented as mean ± SEM; Ordinary one-way ANOVA test was used for panels A,D and *t*-test two-sided in panel B comparing each time with their respective untreated control; significance levels are indicated as follows: *p < 0.05; **p < 0.0021; ***p < 0.0002; ****p < 0.0001; *ns* indicates no significant difference (p > 0.05). Source data are provided as a Source Data file.

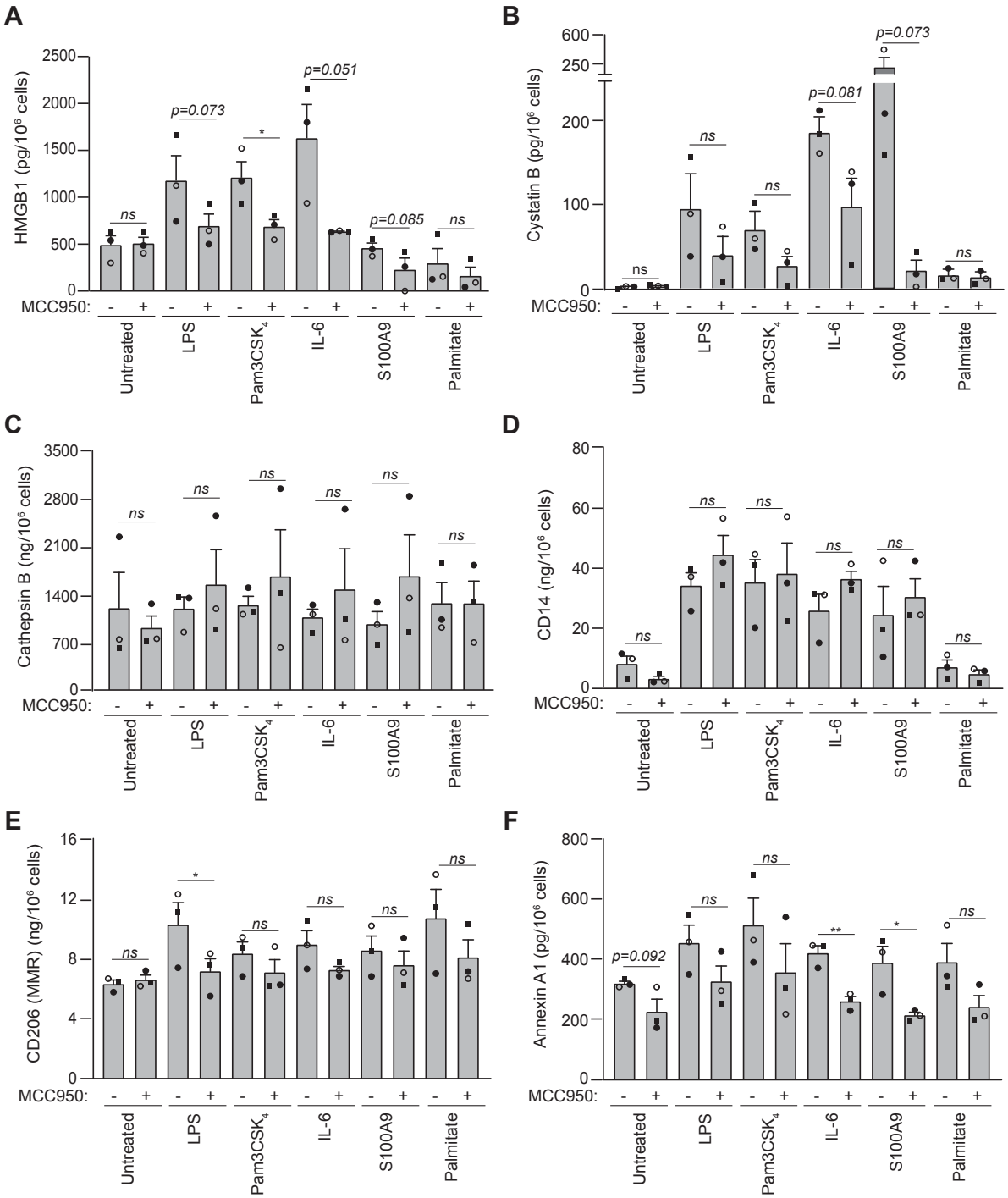

Supplementary Figure 4. Secretome of CAPS-associated NLRP3 variants.
(**A-F**) ELISA for the release of HMGB1 (A), cystatin B (B), cathepsin B (C), soluble CD14 (D), soluble CD206 (E) or annexin A1 (F) from *Nlrp3*$^{-/-}$ immortalized macrophages expressing the human NLRP3 p.D303N variant induced after 16 h treatment with doxycycline (1 µg/ml) and palmitate (1 mM), recombinant S100A9 (0.5 µg/ml), recombinant IL-6 (0.5 µg/ml), LPS (0.1 µg/ml) or Pam3-CSK_4 (1 µg/ml), in the absence or presence of MCC950 (10 µM).
Graphics are representative of *n*= 3 independent experiments (each one represented by a different symbol) and data is represented as mean ± SEM; *t*-test two-sided was used to compare the effect of MCC950 for each NF-κB inducer; significance levels are indicated as follows: *p < 0.05;**p < 0.0021; *ns* indicates no significant difference (p > 0.05). Source data are provided as a Source Data file.

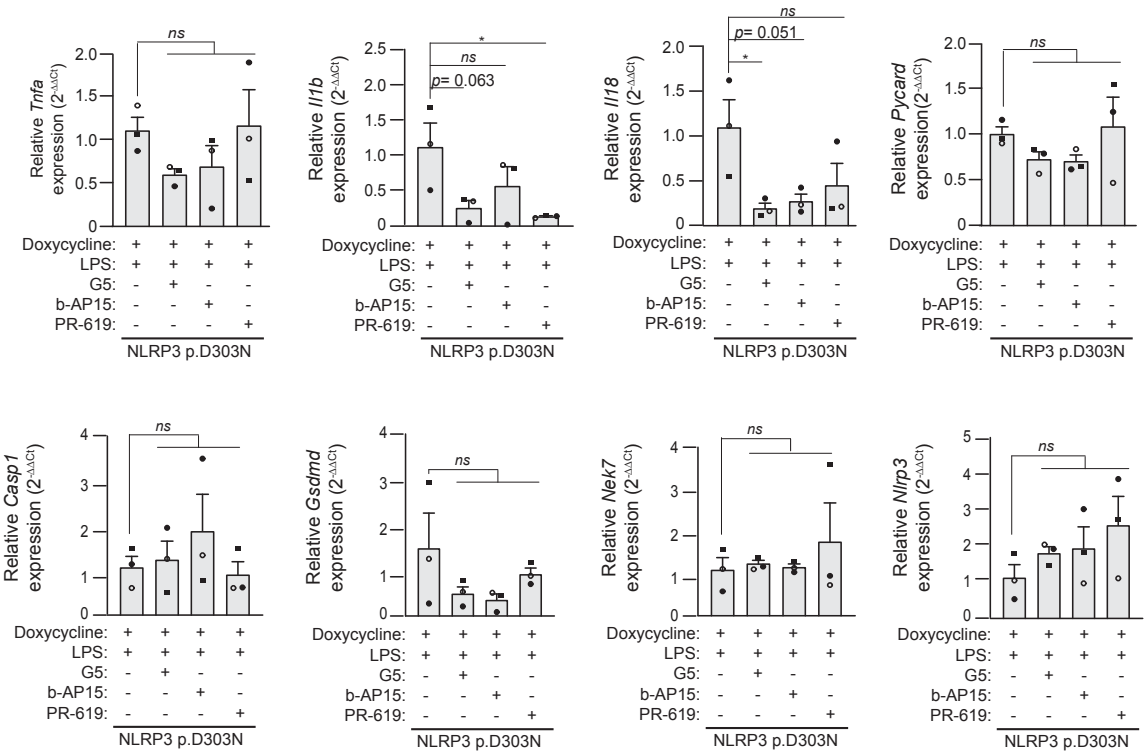

Supplementary Figure 5. Deubiquitinases inhibitors affect the expression of *Il1b*, *Il18*, but not the expression of other inflammasome components or *Tnfa*.
Gene expression ($2^{-\Delta\Delta Ct}$) relative to doxycycline and LPS treatment for *Tnfa*, *Il1b*, *Il18*, *Pycard*, *Casp1*, *Gsdmd*, *Nek7* and *Nlrp3* from *Nlrp3*$^{-/-}$ immortalized macrophages expressing the human NLRP3 p.D303N mutant induced after 16 h treatment with doxycycline (1 µg/ml) and then treated for 6 h with LPS (100 ng/ml), with or without G5 (5 µM), b-AP15 (5 µM) or PR-619 (10 µM).
Graphics are representative of *n*= 3 independent experiments (each one represented by a different symbol) and data is represented as mean ± SEM; Ordinary one-way ANOVA test was used; significance levels are indicated as follows: *p < 0.05; *ns* indicates no significant difference (p > 0.05). Source data are provided as a Source Data file.

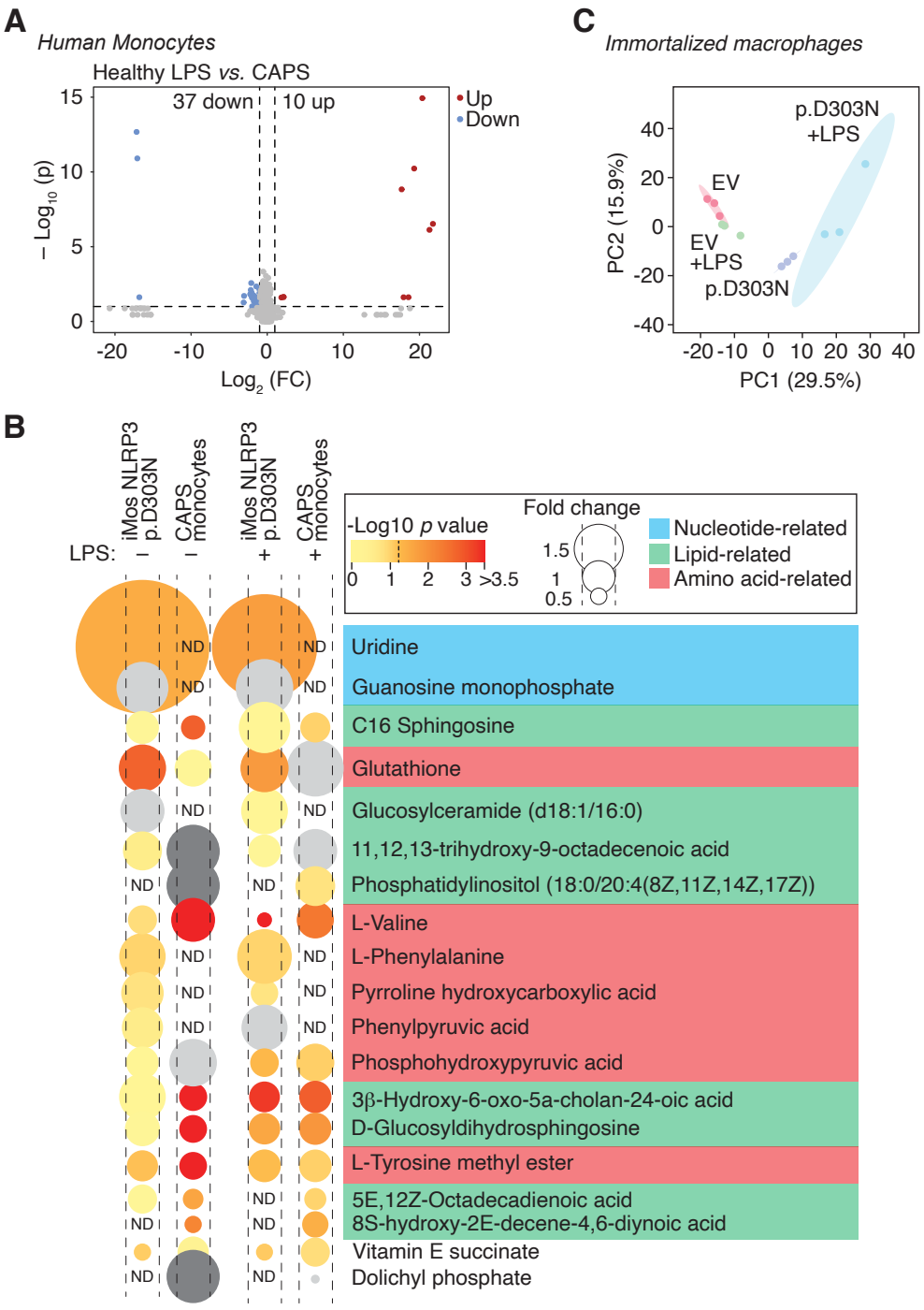

Supplementary Figure 6. Immunometabolism of myeloid cells expressing CAPS-associated NLRP3 variants

(**A**) Volcano plot of metabolites present in blood monocytes from healthy subjects (*n*= 4) and CAPS patients (*n*= 4), with expression (log_2 values) plotted against the adjusted P value for the difference in metabolite abundance; *t*-test two-sided. Metabolites that are significantly upregulated (red) or downregulated (blue) by one-fold or more in monocytes from CAPS patients are compared to those in monocytes from healthy subjects treated for 2 h with LPS (500 ng/ml).

(**B**) Abundance profile of metabolites tentatively identified in human CAPS monocytes (*n*= 4) and iMos expressing human NLPR3 p.D303N (*n*= 3) after treatment with doxycycline, both with or without LPS as in panels A and C respectively. Metabolites were grouped based on their properties: nucleotide-related (blue), lipid-related (green)

and amino acids-related (pink). The data are represented as circles, where the size indicates the fold change relative to healthy donor monocytes or iMos without doxycycline treatment, and the colour represents the $-Log_{10}$ *p*-value (the dotted line in the colour scale represents $p = 0.05$; *t*-test two-sided). Light grey indicates insufficient power to calculate statistics, while dark grey indicates that the metabolite was not detected in heathy donor monocytes and only in CAPS samples. ND denotes not detected.
(**C**) Principal component analysis (PCA) model of metabolomic profiles of *Nlrp3*$^{-/-}$ immortalized macrophages (iMos) expressing human NLRP3 p.D303N or not (empty vector, EV), treated with doxycycline (1 µg/ml) for 16 hours and then for 4 h with or without LPS (100 ng/ml) ($n = 3$). Source data are provided as a Source Data file.

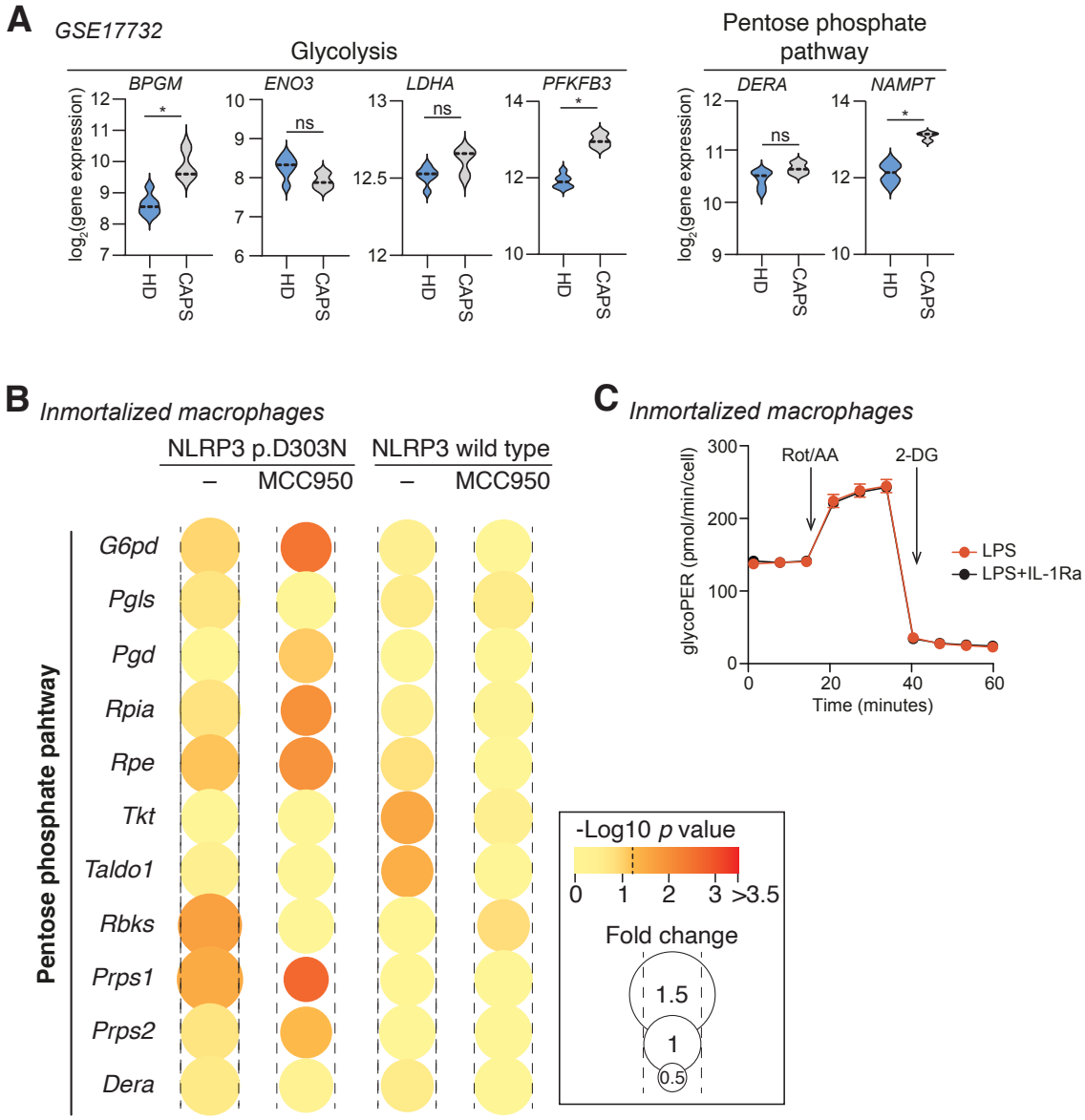

Supplementary Figure 7. Comparative analysis of gene expression in cells with CAPS-associated NLRP3 variants

(**A**) Glycolysis and pentose phosphate pathway gene expression in blood cells from healthy donors (HD, *n*= 6) and CAPS patients during active disease (*n*= 3) was represented as violin plot (using dataset GSE17732). The median is represented by the middle dotted line. Data were analysed using a *t*-test two-sided with Benjamini–Hochberg correction to compare gene expression. * denotes $p< 0.05$, while *ns* indicates no significant difference ($p> 0.05$).

(**B**) Relative expression of pentose phosphate pathway genes in *Nlrp3*$^{-/-}$ immortalized macrophages (iMos) treated for 16 h with or without doxycycline (1 µg/ml) to induce the expression of the human NLRP3 wild type or the p.D303N variant, in the absence or presence of MCC950 (10 µM). The data are represented as circles, where the size indicates the fold change of doxycycline treated cells vs untreated cells, or the fold change of doxycycline with MCC950 treatment vs doxycycline, and the colour represents the $-\text{Log}_{10}$ *p*-value (the dotted line in the colour scale represents $p= 0.05$); *t*-test two-sided. The graphics represent data from three to four independent experiments.

(**C**) Seahorse analysis of glycolysis in *Nlrp3*$^{-/-}$ iMos treated for 16 h with doxycycline (1 µg/ml) to induce the expression of the human NLRP3 p.D303N variant and LPS (100 ng/ml), in the absence or presence of IL-1Ra (100 ng/ml). The data are derived from 4 biological replicates, which are representative of 2 independent experiments. Source data are provided as a Source Data file.

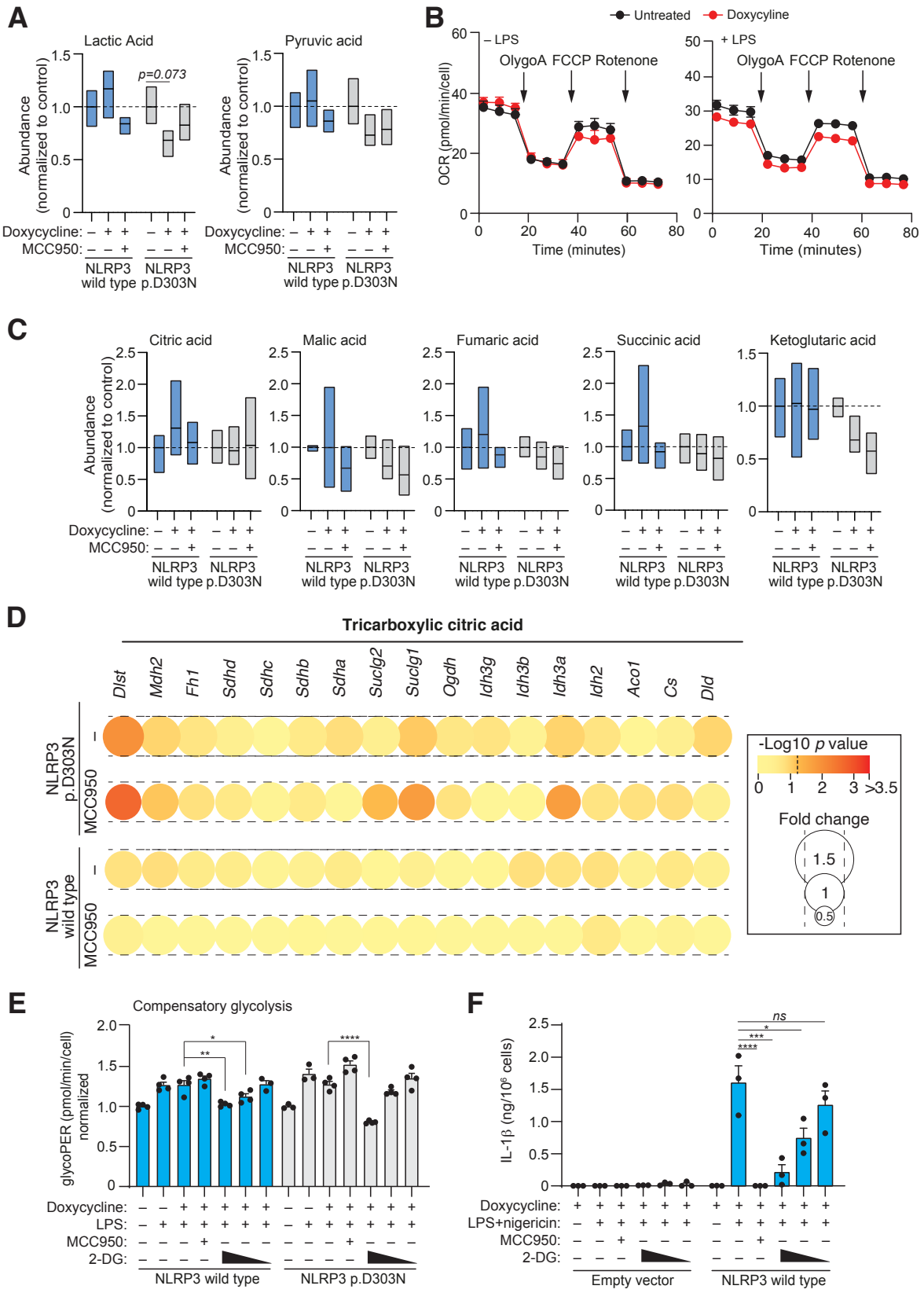

Supplementary Figure 8. Metabolic reprogramming in macrophages expressing the NLRP3 p.D303N variant

(**A**) Normalized abundance of lactic acid and pyruvic acid in *Nlrp3*$^{-/-}$ immortalized macrophages (iMos) expressing either the wild type NLRP3 or the p.D303N variant,

treated for 16 h with or without doxycycline (1 µg/ml) and MCC950 (10 µM). The graphics represent the data from *n*= 3 independent experiments, with the median indicated by the middle line. The dotted line represents the abundance level in control cells.

(**B**) Seahorse analysis of mitochondria oxygen consumption rate (OCR) in iMos treated for 16 h with or without doxycycline (1 µg/ml), in the absence (left) or presence (right) of LPS (100 ng/ml). The data represent 8 biological replicates, and is representative from three independent experiments.

(**C**) Normalized abundance of various metabolites of the tricarboxylic citric acid (TCA) cycle in iMos treated as described in panel A. The graphics are representative of three independent experiments, with the median indicated by the middle line. The dotted line represents the abundance level in control cells.

(**D**) Relative expression of TCA genes from iMos treated as described in panel A. The data are represented as circles, where the size indicates the fold change of doxycycline treated cells vs untreated cells, or the fold change of doxycycline with MCC950 treatment vs doxycycline, and the colour represents the $-\text{Log}_{10}$ *p*-value (the dotted line in the colour scale represents *p*= 0.05). The graphics represent data from three to four independent experiments.
(**E**) Compensatory glycolysis of iMos treated as described in panel A, but for 4 h and with 2-deoxy-D-glucose (2-DG, at different concentrations 0.1, 0.5 and 1 mM). The data represent 3-4 biological replicates, and is representative from two independent experiments.

(**F**) ELISA for IL-1β release from iMos expressing or not wild type NLRP3 treated for 4 h with doxycycline (1 µg/ml), MCC950 (10 µM), LPS (100 ng/ml) or 2-DG (0.1, 0.5 and 1 mM), and then treated for 30 min with nigericin (10 µM) (*n*= 3).

For panels B,E,F data are represented as mean ± SEM, for panels A,C data are represented as mean (middle line) and bounds of box represent the 25^{th} to 75^{th} percentile respectively; Ordinary one-way ANOVA test was used for panel E,F, and *t*-test two-sided was used for panels A,D; *p < 0.05; **p < 0.0021; ***p < 0.0002; *ns*, no significant difference (p > 0.05). Source data are provided as a Source Data file.

SUPPLEMENTARY TABLES

Supplementary Table 1. Demographic and clinical information of the individuals enrolled in this study.

	Healthy controls	CAPS
N	9	7
Age in years, mean (range) ± SD	32.89 (23-44) ± 8.13	51.85 (20-73) ± 17.45
p value		*p*= 0.011
Gender, N (%)		
Male	3 (66.6)	5 (71.4)
Female	6 (33.3)	2 (28.6)
p value		*p*= 0.131^{ns}
Clinical data *(only for CAPS patients)*		
NLRP3 variant, N (%)		
p.D303N		1 (14.3)
p.R260W		1 (14.3)
p.T348M		1 (14.3)
p.A439T		4 (57.1)
Clinical phenotype, N (%)		
MWS		6 (85.7)
MWS/CINCA		1 (14.3)
Treatment, N (%)		
Canakinumab		3 (42.9)
Anakinra		4 (57.1)

CINCA: chronic infantile neurologic cutaneous articular syndrome; MWS: Muckle–Wells syndrome; *ns*, no significant difference (p> 0.05); SD, standard deviation

Chi-square (χ^2) test was used for gender and *t*-test two-sided was used for age.

Supplementary Table 2. Tentative identification of metabolites in human monocytes that are differentially present in CAPS monocytes.

Metabolite	Formula	Mass	Polarity	error (ppm)	Fold change untreated	Fold change LPS
Glutathione	$C_{10}H_{17}N_3O_6S$	307.084	Pos	0.63	1.04	1.60
11,12,13-trihydroxy-9-octadecenoic acid	$C_{18}H_{34}O_5$	330.2406	Neg	-1.73	ND in untreated HD monocytes, only in CAPS	1.35
Phosphatidylinositol (18:0/20:4(8Z,11Z,14Z,17Z))	$C_{47}H_{83}O_{13}P$	886.5573	Neg	-0.43	ND in untreated HD monocytes, only in CAPS	1.22
L-Valine	$C_5H_{11}NO_2$	117.0789	Pos	4.05	1.34* p= 0.0002	1.14* p= 0.004
Phosphohydroxypyruvic acid	$C_3H_5O_7P$	183.9783	Pos	8.52	1.45	1.16
Vitamin E succinate	$C_{33}H_{54}O_5$	530.3978	Pos	7.5	0.96	0.89
3β-Hydroxy-6-oxo-5a-cholan-24-oic acid	$C_{24}H_{38}O_4$	390.2768	Pos	6.5	0.86* p= 5.58^10^{-5}	0.91* p= 0.001
D-Glucosyldihydrosphingosine	$C_{24}H_{49}NO_7$	463.3509	Pos	1.18	0.85* p= 0.0001	0.91* p= 0.013
L-Tyrosine methyl ester	$C_{10}H_{13}NO_3$	195.0899	Neg	-0.68	0.85* p= 1.13^10^{-7}	0.92
Butyl ethyl malonate	$C_9H_{16}O_4$	188.1049	Neg	-2.68	0.82* p= 0.0005	0.94
C16 Sphingosine	$C_{16}H_{33}NO_2$	271.2502	Pos	-1.41	0.74* p= 0.001	0.92
5E,12Z-Octadecadienoic acid	$C_{18}H_{32}O_2$	280.2403	Pos	2.21	0.63* p= 0.021	0.67
8S-hydroxy-2E-Decene-4,6-diynoic acid	$C_{10}H_{10}O_3$	178.0631	Pos	3.7	0.53* p= 0.0079	0.81* p= 0.034
Dolichyl phosphate	$C_{25}H_{45}O_4P$	440.306	Pos	4.5	ND in untreated HD monocytes, only in CAPS	0.27

Abbreviations: HD: Healthy donor; ND: Non-detected; Neg: negative; Pos: positive; *t*-test two-sided *p<0.05.

Supplementary Table 3. Tentative identification of metabolites in immortalized mouse macrophages that are differentially present when NLRP3 p.D303N is expressed.

Metabolite	Formula	Mass	Polarity	error (ppm)	Fold change untreated	Fold change LPS
Uridine	$C_9H_{12}N_2O_6$	244.0697	Neg	0.67	4.09* *p*= 0.03	3.22* *p*= 0.017
Guanosine monophosphate	$C_{10}H_{14}N_5O_8P$	363.0575	Neg	-1.37	1.59	1.76
C16 Sphingosine	$C_{16}H_{33}NO_2$	271.2508	Pos	-1.21	1.01	1.57
Glutathione	$C_{10}H_{17}N_3O_6S$	307.0837	Neg	0.31	1.45* *p*= 0.002	1.47* *p*= 0.016
Glucosylceramide (d18:1/16:0)	$C_{40}H_{77}NO_8$	699.5668	Neg	-2.69	1.24	1.43
11,12,13-trihydroxy-9-octadecenoic acid	$C_{18}H_{34}O_5$	330.241	Neg	1.14	1.10	0.99
L-Valine	$C_5H_{11}NO_2$	117.0789	Pos	-0,67	0.89	0.46* *p*= 3.35^10^{-5}
L-Phenylalanine	$C_9H_{11}NO_2$	165.0787	Pos	-1.69	1.42	1.54
Pyrroline hydroxycarboxylic acid	$C_5H_7NO_3$	129.0424	Neg	-1.5	1.35	0.84
Phenylpyruvic acid	$C_9H_8O_3$	164.0488	Pos	8.87	1.26	1.29
Phosphohydroxypyruvic acid	$C_3H_5O_7P$	183.9784	Pos	6.04	0.96	0.87* *p*= 0.046
3β-Hydroxy-6-oxo-5a-cholan-24-oic acid	$C_{24}H_{38}O_4$	390.2773	Pos	0.74	1.32	0.87* *p*= 0.0004
D-Glucosyldihydrosphingosine	$C_{24}H_{49}NO_7$	463.3513	Pos	0.86	0.99	0.89
L-Tyrosine methyl ester	$C_{10}H_{13}NO_3$	195.0895	Neg	-0.22	0.95	0.92
Butyl ethyl malonate	$C_9H_{16}O_4$	188.1051	Neg	1.28	0.94	0.95
5E,12Z-Octadecadienoic acid	$C_{18}H_{32}O_2$	280.241	Pos	2.75	0.89	ND in LPS-macrophages NLRP3 p.D303N
Vitamin E succinate	$C_{33}H_{54}O_5$	530.3963	Pos	-1.56	0.53	0.52

Abbreviations: ND: Not-detected; Neg: negative; Pos: positive; *t*-test two-sided
*p<0.05.

Supplementary Table 4. Biological processes enriched with upregulated genes upon NLRP3 p.D303N expression.

GO term	Gene count	*p*-value*	Benjamini–Hochberg**	Genes
Inflammatory response (GO:0006954)	30	1.86E-04	0.00944575	*Il1rn, Ddx3x, Dhx9, C5ar1, Hmgb1, Ptgs2, Cxcl2, Tnf, Ccl7, Zc3h12a, Nfkbiz, Ccl2, Ccr7, Cd14, Tnfrsf4, Map2k3, Ccl22, Stard7, Acod1, Ppbp, Tnfrsf1b, Nfkb1, Il17ra, Nfkb2, Cxcl10,*
Positive regulation of apoptotic process (GO:0043065)	30	1.32E-04	0.007331328	*Top2a, Tomm40, Ddx3x, Hmgb1, Ptgs2, Tnf, Hspd1, Ing5, Rassf2, Casp3, C1qbp, Bcl2a1d, Bcl2a1b, Tgm2, Utp11, Ripk2, Txnrd1, Rrp1b, Siah1b, Dhodh, Dnaja1, Nr4a1, Melk, Il1b, Lcn2,*
Steroid metabolic process (GO:0008202)	15	3.12E-4	0.014272545	*Fdps, Hmgcs1, Insig1, Dhcr24, Msmo1, Hmgcr, Srebf2, Cyp51, Nsdhl, Erg28, Chst10, Dhcr7, Ldlr, Lbr, Fdft1*
Cholesterol metabolic process (GO:0008203)	15	5.46E-05	0.003626313	*Fdps, Hmgcs1, Insig1, Lrp5, Dhcr24, Msmo1, Hmgcr, Srebf2, Cyp51, Sqle, Nsdhl, Dhcr7, Ldlr, Lbr, Fdft1*
Response to virus (GO:0009615)	13	1.38E-04	0.00748434	*Ivns1abp, Ifitm3, Ifitm2, Ddx3x, Rsad2, Ddx1, Odc1, Ddx21, Irak3, Tnf, Il17ra, Lcn2, Oasl1*
Steroid biosynthetic process (GO:0006694)	12	2.01E-05	0.001716264	*Fdps, Nsdhl, Erg28, Hmgcs1, Dhcr24, Msmo1, Dhcr7, Hmgcr, Hsd17b7, Lbr, Cyp51, Fdft1*
Cellular response to virus (GO:0098586)	11	1.38E-04	9.55E-04	*Cxcl10, Hsp90aa1, Ddx3x, Tomm70a, Fmr1, Zc3h12a, Gbf1, Rrp1b, Pou2f2, Ikbke, Nfkb1p*
Cellular response to oxidative stress (GO:0034599)	11	0.00106265	0.04040636	*Nr4a2, Chchd4, Pnpt1, Zc3h12a, G6pdx, Gsr, Slc11a2, Atp2a2, Pycr2, Sod2, Eif2s1*
Cellular response to interleukin-17 (GO:0097398)	5	0.00101988	0.039252839	*Cxcl10, Il1b, Srsf1, Nfkbiz, Nfkb1*
Cellular amino acid biosynthetic process (GO:0008652)	4	0.05200478	0.582592119	*Mthfd1, Pycr2, Bcat1, Enoph1*

One-sided *p*-values for Fisher's Exact test* and Benjamini–Hochberg correction for multiple comparisons to obtain *p*-adjusted**.

Supplementary Table 5. Biological processes enriched with downregulated genes upon NLRP3 p.D303N expression.

GO term	Gene count	*p*-value*	Benjamini–Hochberg**	Genes
Lipid metabolic process (GO:0006629)	42	3.1121E-05	0.011874445	*Dgkg, Faah, B4galt1, Cerk, Insig2, Mgst3, Hexb, Hexa, Inppl1, Lpl, Ptpn22, Hacd4, Ptgs1, Pld2, Sult1a1, Hmgcl, Gm2a, Psap, Cyp4v3, Scd2, Pgap6, Inpp5k, Hacl1, Pltp, Hsd3b7, Cpt1a, Gpx1, Sphk2, Sphk1, Nr1h2, Ephx1, Peds1, Plcb3, Soat1, Naaa, Acot2, Rubcnl, Echdc3, Acox3, Pafah1b3, Pam, Slc27a4*
Positive regulation of transcription (GO:0045893)	41	8.7396E-05	0.020332626	*Kdm3a, Calcoco1, Shc1, Cited2, Wbp2, Src, Pbxip1, Rora, Foxo3, Hif1a, Npas2, Phf8, Lbh, Tnni2, Inpp5k, Apbb1, Nos1, Mta3, Trp53inp1, Arhgef11, Arnt2, Egr2, Jun, Niban2, Map3k1, Fzd7, Nr1h2, Tfeb, Dyrk1b, Mitf, Klf4, Usf2, Runx3, Trerf1, Klf2, Mafb, Asph, Id2, Irf8, Mapre3, Map3k12*
Positive regulation of cell migration (GO:0030335)	25	9.0474E-07	6.21E-04	*Grn, Flt1, Cxcr4, Lamc2, Vsir, Gnai2, Pld2, Ppp3ca, Plau, Ccl3, Itgax, S1pr1, C3ar1, Ccr1, Sema4a, Sphk1, Cav1, Sema4g, Vegfa, Cpeb1, Myadm, Numb, Spry2, Myo1f, Bcar1*
Cell proliferation (GO:0008283)	25	9.4735E-05	0.020332626	*Rb1, Rarg, B4galt1, Cited2, Src, Adm, Rasgrp4, Gnai2, Ndst1, S1pr1, Mta3, Tns3, Appl2, Pdk1, Jun, Gpx1, Sphk2, Sphk1, Cav1, Vegfa, Asph, Kitl, Tgfbi, Ypel5, Nodal*
Response to hypoxia (GO:0001666)	23	1.3772E-07	1.58E-04	*Egln1, Arnt2, Camk2d, Cdkn1b, Flt1, Cited2, Cav1, Bnip3, Cxcr4, Adm, Plod1, Hif1a, Vegfa, Pld2, Cd24a, Plau, Ddit4, Acot2, Capn2, Lonp1, Hmox1, Nos1, Pam*
Positive regulation of ERK1, ERK2 cascade (GO:0070374)	20	7.5230E-05	0.020332626	*Ccr1, App, Camk2d, Jun, Shc1, Src, Cxcr4, Trem2, Arrb1, Ptpn22, Mturn, Vegfa, Gnai2, Prxl2c, Nptn, Ccl3, Spry2, Nodal, Map3k12, Mapk3*
Cellular response to hypoxia (GO:0071456)	18	1.2000E-07	1.58E-04	*Egln1, Bnip3l, Src, Bnip3, Trem2, Rora, Ak4, Foxo3, Ndrg1, Hif1a, Rtn4, Vegfa, Cpeb1, Pink1, Rgcc, Eif4ebp1, Hmox1, Mgarp*
Carbohydrate metabolic process (GO:0005975)	17	4.94E-04	0.072104731	*Epm2a, B4galt1, Gbe1, Hexb, Hexa, Pygl, Hexdc, Hk1, Gpi1, Hk3, Ppp1r3c, Hyal1, Ppp1r3b, Gapdh, Pdk2, Pgm1, Pdk1*
Positive regulation of angiogenesis (GO:0045766)	17	1.7689E-05	0.010124058	*Ecm1, Grn, Flt1, Sphk1, Emp2, Adm, Hif1a, Rtn4, Add1, Vegfa, Rhob, Lgals3, Hyal1, C3ar1, Itgax, Hmox1, Nodal*
Actin filament organization (GO:0007015)	16	8.3825E-05	0.020332626	*Tmod1, Gsn, Sh3kbp1, Inppl1, Emp2, Arhgap25, Arhgap6, Rnd3, Mtss1, Coro1b, Rhob, Myo1e, Whamm, Rhoq, Myo1f, Bcar1*

One-sided *p*-values for Fisher's Exact test* and Benjamini–Hochberg correction for multiple comparisons to obtain *p*-adjusted**.